Science of the Total Environment xxx (xxxx) 178379

Contents lists available at ScienceDirect

Science of the Total Environment

journal homepage: www.elsevier.com

Southern California ozone exposure disparities under different emissions control strategies in a low-carbon future

Yusheng Zhao [a], Yin Li [b], Yiting Li [a], Anikender Kumar [b, c], Michael J. Kleeman [b, *]

[a] Department of Land, Air, and Water Resource, University of California, Davis, CA 95616, USA
[b] Department of Civil and Environmental Engineering, University of California, Davis, CA 95616, USA
[c] India Meteorological Department, New Delhi, India

HIGHLIGHTS

- Future adoption of low carbon fuels in Southern California does not eliminate high O_3 concentrations
- Traditional NOX control programs to control O_3 would exacerbate race-based exposure disparities
- Tools developed for NOx and O_3 source apportionment can be adapted to calculate sources contributing to exposure disparities
- The Los Angeles International Airport (LAX) contributes most strongly to future race-based exposure disparities for NO_2 in Southern California

GRAPHICAL ABSTRACT

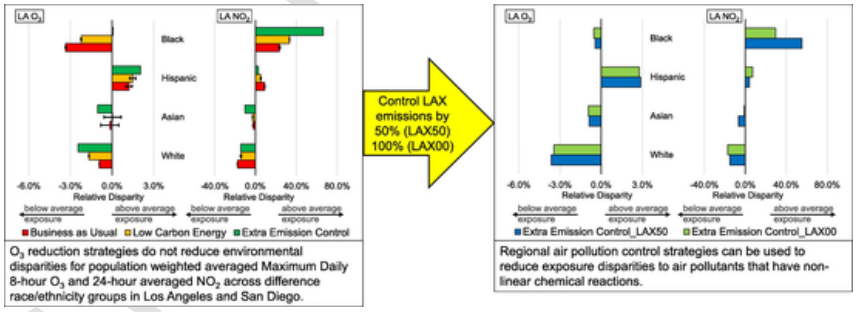

O_3 reduction strategies do not reduce environmental disparities for population weighted averaged Maximum Daily 8-hour O_3 and 24-hour averaged NO_2 across difference race/ethnicity groups in Los Angeles and San Diego.

Regional air pollution control strategies can be used to reduce exposure disparities to air pollutants that have non-linear chemical reactions.

ARTICLE INFO

Editor: Hai Guo

Keywords:
Environmental justice
Exposure disparity
Ozone
Ozone source apportionment
NOx control
CTM

ABSTRACT

Environmental justice (EJ) has emerged as a critical consideration when planning new air pollution control strategies. In this study we analyze how traditional ozone (O_3) control strategies for the year 2050 will affect exposure disparities, defined as departures from the population average exposure, for O_3 and oxides of nitrogen (NOx) in Southern California. Future air quality fields were simulated using a chemical transport model under five emission scenarios that explore a range of traditional controls that target the largest sources of precursor emissions using a novel O_3 source apportionment technique but without considering exposure disparities. We find that traditional O_3 control strategies reduce O_3 exposure disparities by <1.6 % and reduce NO_2 exposure disparities by <9 % in Southern California. For the Black and African residents living in the urban core of Los Angeles, the relative NO_2 exposure disparities increase from $+23.1$ % to $+66.2$ % and O_3 exposure disparities increase from -3.3 % to $+0.1$ % due to NOx emissions reductions mainly in outlying regions and the NOx-rich environment in the urban core. Additional analysis shows that complete elimination of NOx emissions from Los Angeles International Airport (LAX) would reduce the NO_2 exposure disparities by up to 50 %, but there is currently no practical method to achieve this goal. The results of the current study highlight the challenge of simultaneously attaining O_3 standards and reducing exposure disparities for O_3 and NO_2 in cities with NOx-rich urban cores. Reducing emissions by region may be a solution to this challenge.

* Corresponding author.
E-mail address: mjkleeman@ucdavis.edu (M.J. Kleeman).

https://doi.org/10.1016/j.scitotenv.2025.178379
Received 9 July 2024; Received in revised form 31 December 2024; Accepted 2 January 2025
0048-9697/

1. Introduction

Despite decades of control efforts, ambient air pollution persists as one of the greatest environmental threats to global human health, causing an estimated 4.2 million premature deaths in 2019 alone (World Health Organization, 2022). In the United States, concentrations of criteria air pollutants have declined significantly over the past five decades, bringing most of the U.S. territories into compliance with National Ambient Air Quality Standards (NAAQS). Despite this progress, residual air pollution problems exist, and they do not affect all U.S. residents equally, especially for ground-level ozone (O_3) (Collins et al., 2022; Miranda et al., 2011; Pope et al., 2016). In 2023, the national average of Fourth Daily Max 8-hour O_3 was 69 ppb among 484 national sites, with a maximum value of 107 ppb, and with 189 sites exceeding the 70-ppb NAAQS (U.S. EPA, 2024a, 2024b). The spatial pattern of air pollution combined with historical housing practices and present-day socio-economic factors results in higher air pollution exposures in minority communities, causing environmental disparities including higher health risks (Anderson et al., 2018; Bluhm et al., 2022; Cushing et al., 2015; Lane et al., 2022; Liu et al., 2021; Miranda et al., 2011; Morello-Frosch et al., 2002; Tessum et al., 2021).

Many studies have emphasized that environmental justice (EJ) must be considered when new air quality control strategies are designed (Anderson et al., 2018; Boyce and Pastor, 2013; Gallagher and Holloway, 2022; Mitchell et al., 2015; Morelli et al., 2019; Picciano et al., 2023; Wang et al., 2023a). This is especially important for California, as a state with the second highest racial diversity index in the U.S. (U.S. Census Bureau, 2021). EJ has been defined by the United States Environmental Protection Agency (US EPA) as the fair treatment and meaningful engagement of all people, regardless of income, race, color, national origin, tribal affiliation, or disability, during the process of agency decision-making and any federal activities that could impact human health and the environment (U.S. EPA, 2024b). When EJ is properly incorporated into environmental regulations, people will be fully protected from disproportionate and adverse human health and environment risks and hazards, and have equitable access to a healthy, sustainable, and resilient environment.

Previous studies have focused on EJ analysis of particulate matter (PM), O_3, and nitrogen dioxide (NO_2), but most of these studies focus on past years (Bravo et al., 2016; Colmer et al., 2020; Kheirbek et al., 2013; Li et al., 2022a; Mitchell and Dorling, 2003). A few studies look at the future EJ, but only for PM (Li et al., 2022b; Luo et al., 2022; Picciano et al., 2023). Meanwhile, many studies have analyzed the impact of certain emission sources and locations on EJ (Do et al., 2021; Goodkind et al., 2019; Houston et al., 2004; Li et al., 2022b; Nguyen and Marshall, 2018; Shah et al., 2020; Thind et al., 2019), but these studies generally didn't use source apportionment methods to identify sources of O_3 exposure disparities. Wang et al. (2022) used a source-receptor matrix in their model to estimate the optimized emission sectors for reduction to minimize the $PM_{2.5}$ exposure disparities, but their model was not able to predict O_3 (Tessum et al., 2017). More studies are needed to explore future O_3 exposure disparities and disparity reduction strategies.

California is transitioning to low carbon fuels in direct response to climate change, but these measures will also influence concentrations of traditional air pollutants such as O_3. The regulations and bills designed to reduce greenhouse gas (GHG) emissions 80 % below 1990 levels by the year 2050 (California Air Resources Board, 2006) will also reduce concentrations of $NO + NO_2$ ($= NOx$), which is a precursor to O_3 formation. O_3 chemistry is complex and nonlinear, meaning that NOx reductions in urban cores can lead to higher O_3 concentrations (Wu et al., 2024, 2022; Zapata et al., 2018a; Zhao et al., 2024). However, previous studies have shown that the majority of VOC emissions in Southern California that contribute to O_3 formation are biogenic emissions (Pfannerstill et al., 2024; Wu et al., 2024; Zhao et al., 2024), which makes it difficult to control O_3 by reducing VOC emissions. To avoid the increased O_3 due to NOx reductions, a deep cut in NOx emissions would be necessary, i.e. >40 % as suggested by Wu et al. (2024). Supplemental controls were designed to offset this unintended increase in O_3 concentrations for the year 2050 (Zhao et al., 2024) but the EJ aspects of these strategies need further study.

Here we analyze the environmental disparities related to O_3 and NO_2 exposures for the year 2050 after the adoption of low carbon energy and supplemental measures (Li et al., 2022b; Zapata et al., 2018a) that were previously established in Zhao et al. (2024) to achieve compliance with the O_3 NAAQS in the South Coast Air Basin (SoCAB). We also analyze the environmental disparities for historical periods between 2000 and 2019 for comparison. We use a 3-D chemical transport model (CTM) to simulate the air quality for the past two decades and future scenarios with reduced GHG emissions (Li et al., 2022b; Zapata et al., 2018a). An O_3 source apportionment technique is applied to help design supplemental O_3 control strategies that can achieve compliance with the O_3 NAAQS in the future. Exposure disparities under each future scenario are analyzed for race/ethnicity groups defined by the American Community Survey (ACS). The issues that cause residual exposure disparities are discussed and future strategies to reach exposure equity for all race/ethnicity groups are explored.

2. Methods

2.1. Air quality simulations

2.1.1. Model description

Air quality fields were simulated using the University of California Davis/California Institute of Technology (UCD/CIT) air quality model. The UCD/CIT model is a research CTM model that has robust model performance statistics (Hu et al., 2015; Venecek et al., 2019, 2018b;

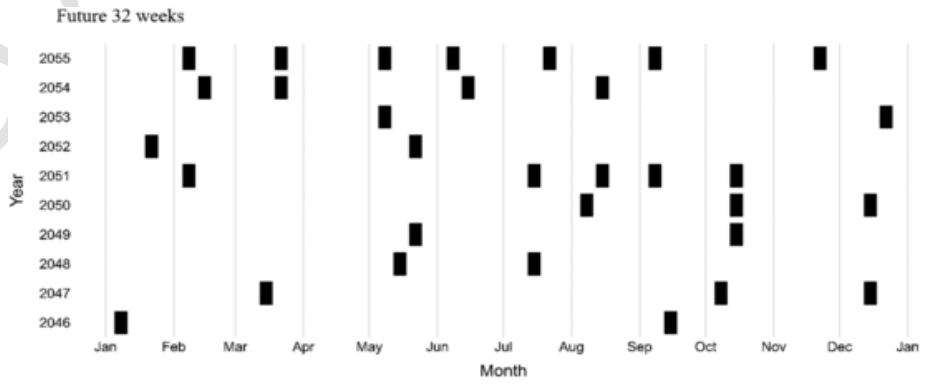

Fig. 1. Selected 32 weeks during the 10-year period. Each black bar indicates a selected week.

Table 1
Regulatory compliance future emission scenario description.

Scenario	Description
BAU	A "business-as-usual" case where greenhouse gas emissions in 2020 are reduced below 1990 levels but no more constraints beyond 2020 under current California's regulations
GHGAi	A climate-friendly greenhouse gas reduction case that achieved California's climate goal of 80 % reduction of GHG emissions relative to 1990 levels by the year 2050 with adoption of advanced technologies and renewable energies
GHGAi_ControlStepI	An emission reduction scenario based on GHGAi scenario that reduced 100 % of all pollutant emissions from "off-road equipment & rail" and 80 % NOx emissions from "marine vessels"
GHGAi_ControlStepII	An emission reduction scenario based on GHGAi scenario that reduced 100 % of all pollutant emissions from "off-road equipment & rail", 80 % NOx emissions from "marine vessels", and 50 % NOx emissions from "industry and agriculture"
GHGAi_ControlStepIII	An aggressive emission reduction scenario based on GHGAi scenario that reduced 100 % of all pollutant emissions from "off-road equipment & rail", 90 % NOx emissions from "marine vessels", and 100 % NOx emissions from "industry and agriculture"

Table 2
Model performance statistics of MD8H O_3 at selected EPA sites for 2000–2009 and 2010–2019 periods.

	2000–2009			2010–2019		
	NMB	NME	r	NMB	NME	r
060371103 Los Angeles	5.12 %	25.76 %	0.778	7.58 %	24.44 %	0.650
060658001 Riverside	−1.76 %	19.95 %	0.809	−0.11 %	20.28 %	0.688
060372005 Pasadena	3.29 %	23.89 %	0.786	8.18 %	20.88 %	0.667
060714003 Redlands	2.43 %	19.53 %	0.829	−1.33 %	17.95 %	0.756

Ying et al., 2008; Yu et al., 2019; Zhao et al., 2022). In the current study, the UCD/CIT model was configured with a flexible O_3 source apportionment technique that enables O_3 tagging for NOx and VOC sources (Zhao et al., 2022). The source tagging technique can quantify the contributions of emissions from different geographical regions to concentrations in other geographical regions (Ying and Kleeman, 2006) or emissions from different source sectors to the concentrations at receptor locations (Cohan and Napelenok, 2011; Ying et al., 2004). In this study, we only analyzed the contributions of emissions from different source sectors. The SAPRC11 chemical mechanism (Carter and Heo, 2013) was used to describe the gas-phase chemical reactions in the UCD/CIT model. Previous studies show that SAPRC11 has superior performance when predicting O_3 in California compared to SAPRC16 (Venecek et al., 2018a), which is very similar to the most recent SAPRC22 mechanism. The SAPRC11 chemical mechanism was configured two ways, one way enabling O_3 apportionment from NOx sources (NOx SA) and the second way enabling O_3 apportionment from VOC sources (VOC SA). NOx SA tags the nitrogen atom in NOx and NOx reaction products, including NO_3, N_2O_5, HNO_3, HNO_4, PAN, etc. VOC SA tags the odd oxygen in all VOC species. Both methods tag the species involved in the primary photolytic cycle, including O^3P, O^1D, and O_3.

2.1.2. Simulation domain and periods

Air quality was simulated for two domains that covered the state of California with a resolution of 24 km, and Southern California with a resolution of 4 km (Fig. S1). This study focuses on the 4-km Southern California domain. Simulations were conducted over three 10-year periods. The first two periods from 2000 to 2009 and 2010 to 2019 establish a historical context for air pollution exposure in California. The future 32-week period spans from 2046 to 2055 to analyze upcoming air quality issues and to develop effective control strategies. The sample subset of 32 weeks (Fig. 1) was randomly selected from 2046 to 2055 to properly represent inter-annual variability associated with the El Nino Southern Oscillation (ENSO) cycle, which is the dominant mode of inter-annual climate variability that affects regional climate and air quality in California (Lin et al., 2015; Xu et al., 2017; Zhang et al., 2012). Eight weeks were selected in each of the four seasons to ensure representative coverage throughout the year, with each week having extra four days for spin-up time (total of 11 days simulated for each week). This sampling approach characterizes both the long-term average and the variability (Table S1) in pollutant concentrations, yielding standard deviations (std_devs) of BAU and GHGAi concentrations under RCP8.5 that are comparable with the std_devs of concentrations predicted for the years 2010–2019. The approach balances accuracy with computational efficiency that avoids simulating every day in the 10-year window. The uncertainty associated with this 32-week sampling approach is discussed in the following section.

2.1.3. Meteorological fields

Meteorology inputs for the CTM were generated by the Weather Research and Forecasting (WRFv3.4) model. The periods 2000–2009 and 2010–2019 used initial/boundary conditions from NCEP North American Regional Reanalysis (NARR) (National Centers for Environmental Prediction et al., 2005). The future 32-week period used initial/boundary conditions from the Community Earth System Model (CESM) (Research Data Archive et al., 2011) under the representative concentration pathway (RCP) 8.5, an upper-bound high GHG-emissions scenario, and the intermediate RCP4.5 scenario described by the Intergovernmental Panel on Climate Change (IPCC). The RCP8.5 was chosen as the focus of this study to analyze worst-case climate scenario for the feasibility of O_3 control strategies. A recent study has shown that RCP8.5 is the best match to the midcentury under current policies (Schwalm et al., 2020). The RCP4.5 sensitivity study was used in combination with two California emissions scenarios to analyze the impacts of alternative climate scenarios on EJ. Four-dimensional data assimilation (FDDA) was used in 2000–2009, and 2010–2019 periods, but not in the future 32-week period. The FDDA used the NCAR ADP observation database (National Centers for Environmental Prediction et al., 2004a, 2004b, 1980a, 1980b) with the global CFSR model data (Saha et al., 2014, 2010) quality control checked as background.

2.1.4. Emissions

Five future emission scenarios for criteria pollutants in the state of California were simulated in this study (see Table 1). Emissions in each scenario were grouped into nine source sectors: "tire and break wear", "on road vehicles", "off-road equipment and rail", "marine vessels and aircraft", "residential and commercial buildings", "electricity generation", "fuel supply", "industrial and agricultural", and "biogenic emissions". Two emission scenarios, "business-as-usual" (BAU) scenario and "greenhouse gas reduction" (GHGAi) scenario were previously constructed using the energy-economic optimization model, CA-TIMES, combined with the California Regional Multisector Air Quality Emissions (CA-REMARQUE_v1.0) model (Li et al., 2022; Zapata et al., 2018b). In the BAU scenario, GHG emissions are reduced to 1990 levels. In the GHGAi scenario, GHG emissions are reduced 80 % below 1990 levels in the most economical manner possible in order to achieve California's climate goal (California Air Resources Board, 2006). Each GHG emissions scenario was translated to a criteria pollutant emissions scenario using CA-REMARQUE. Three additional criteria pollutant control scenarios were constructed based on the GHGAi scenario in order to reduce O_3 concentrations in SoCAB in the year 2050 to comply with the O_3 NAAQS (Zhao et al., 2024). The three GHGAi control scenarios reduced the emissions cumulatively, with GHGAi_ControlStepI being least stringent and GHGAi_ControlStepIII being most stringent. GHGAi_ControlStepI reduced 100 % of all pollutant emissions from "off-

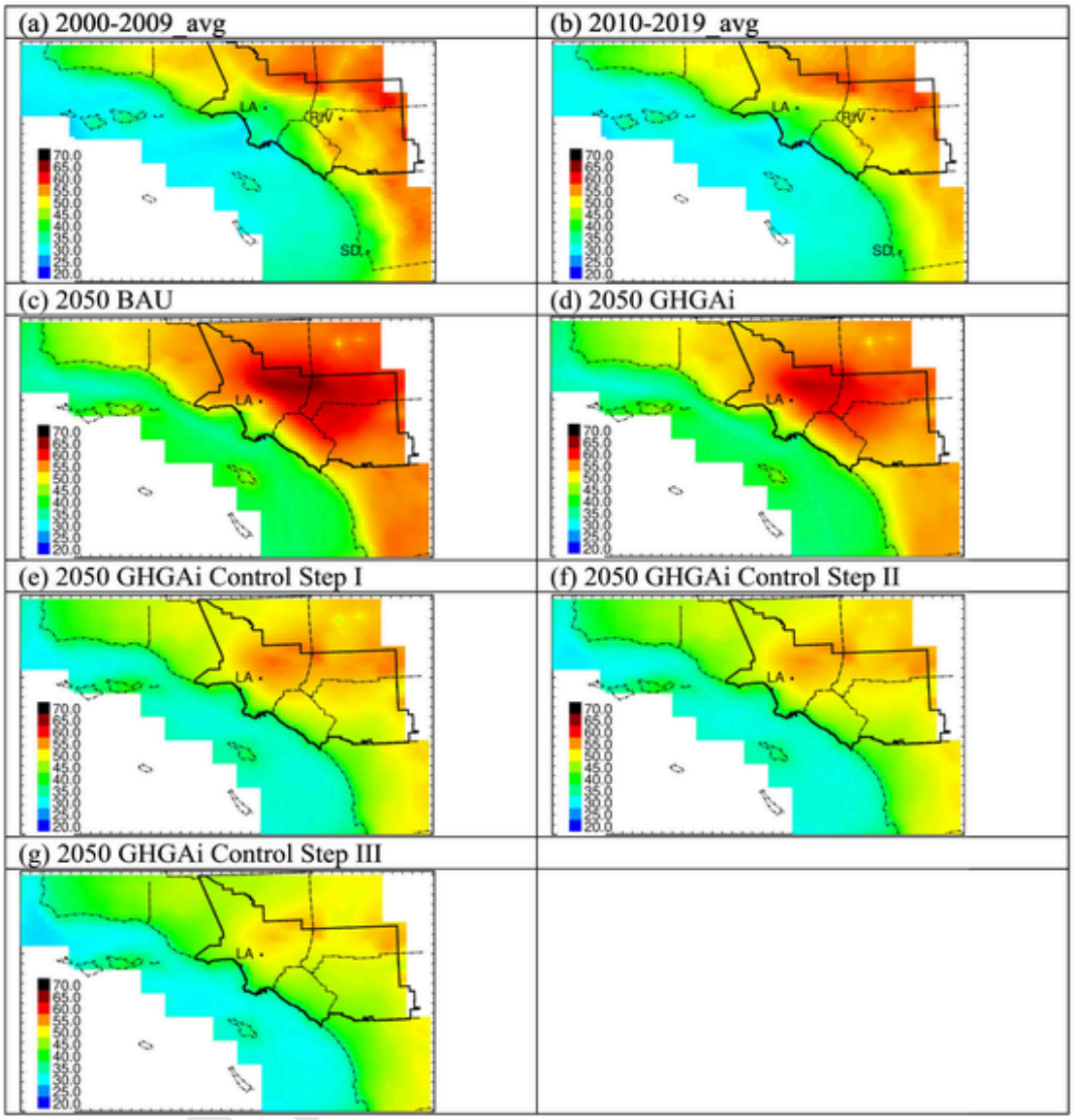

Fig. 2. MD8H O_3 concentrations averaged across 2000–2009, 2010–2019, and the future 32-week simulation period under RCP8.5. Bold line indicates border of the SoCAB. (All concentrations in units of ppb).

road equipment & rail" by assuming adoption of clean energy that has zero emissions, and 80 % NOx emissions from "marine vessels" in compliance with the International Convention for the Prevention of Pollution from Ships (MARPOL) Annex VI Tier III standard. In addition to the emission reductions in GHGAi_ControlStepI, GHGAi_ControlStepII further reduced 50 % of the NOx emissions from "industry and agriculture" through the adoption of low-NOx engines. GHGAi_ControlStepIII used more clean energy and applied more aggressive controls than the previous two control measures, with 100 % of all pollutant emissions eliminated from "off-road equipment & rail", 90 % of the NOx emissions eliminated from "marine vessels", and 100 % of the NOx emissions eliminated from "industry and agriculture". All five future emission scenarios were analyzed under meteorology from the RCP8.5 scenario, while the BAU and GHGAi emission scenarios were additionally analyzed under the RCP4.5 climate scenario as a sensitivity study. Hereafter, all mention of "BAU" and "GHGAi" refers to the BAU and GHGAi scenarios coupled with RCP8.5 unless otherwise noted. Figs. S2 and S3 show the annual average NOx and NMVOC emissions (tons per day) in GHGAi and the reductions in different Control Steps compared to GHGAi. Table S2 shows the population weighted annual total emissions (tons per year) in LA and SD under GHGAi and the percentage of change in different Control Steps compared to GHGAi. Anthropogenic emissions during the 2000–2009 and 2010–2019 historical periods were generated using the Sparse Matrix Operator Kernel Emissions (SMOKEv3.7) modeling system with the California Air Resource Board (CARB) emission inventories. Biogenic emissions for the three 10-year periods were generated using the Model of Emissions of Gases and Aerosols from Nature (MEGANv2.1) based on daily meteorological inputs from WRF.

2.1.5. Initial and boundary conditions

Predictions from the Model for Ozone and Related chemical Tracers (MOZART) for 2000–2015 and the Community Atmosphere Model with Chemistry (CAM-chem) for 2016–2019 were used as the initial and boundary conditions for air quality simulations from 2000 to 2019. For the year 2050, we assumed that the initial and boundary conditions would be similar to current conditions adjusted for seasonality. There-

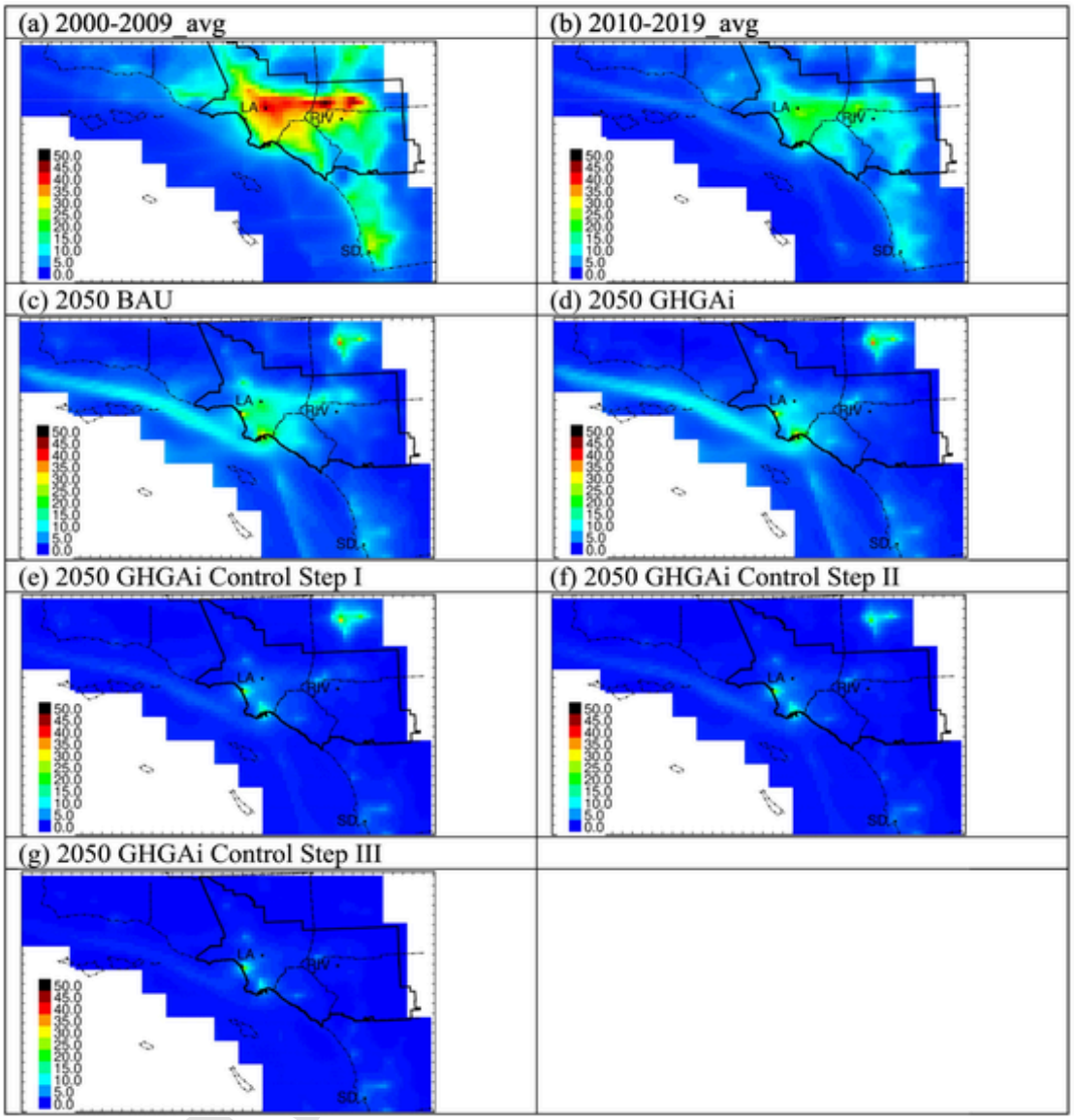

Fig. 3. 24hr-avg NO_2 concentrations averaged across 2000–2009, 2010–2019, and the future 32-week simulation period under RCP8.5. Bold line indicates border of the SoCAB. (All concentrations in units of ppb).

fore, initial and boundary conditions for 2046–2055 used MOZART predictions for the same day of the year in the range 2000–2009.

2.2. Environmental disparity

Race and ethnicity information was obtained from the American Community Survey (ACS) 2012–2016 dataset (U.S. Census Bureau, 2020) that includes Black and African Americans (Black), Hispanic or Latino (Hispanic), Asian, and non-Hispanic or non-Latino White (White) people at the census tract level. Fig. S4 shows the two geographic regions in Southern California used in this calculation: Los Angeles (LA) and San Diego (SD). The population data by race/ethnicity group in the LA and SD regions is shown in Table S3. Estimates of changing future demographics are highly uncertain, and so present-day population demographics are used for all calculations.

Environmental disparity was calculated using population weighted average concentrations for 4KM results for two air pollutants: maximum daily 8-h average (MD8H) O_3 and 24 h-averaged (24 h-avg) NO_2. The population weighted average is a good proxy for the exposure for a whole race/ethnicity group and enables racial equity comparison (Gallagher and Holloway, 2022; Lane et al., 2022; Li et al., 2022b; Liu et al., 2021; Picciano et al., 2023; Tessum et al., 2021; Wang et al., 2023b). This approach does not consider the total numbers of exposed people in each race/ethnicity group since each race/ethnicity group should be treated fairly, regardless of size. Both pollutants were averaged across 2000–2009 (2000–2009_avg), 2010–2019 (2010–2019_avg), and future 32 weeks under different emission scenarios. Average pollutant exposures for each race/ethnicity group were calculated using the equation:

$$C^{k}_{pop-wgted} = \frac{\sum_{(i,j)=(1,1)}^{(imax,jmax)} C_{i,j} P^{k}_{i,j}}{\sum_{(i,j)=(1,1)}^{(imax,jmax)} P^{k}_{i,j}}$$

where: $C^{k}_{pop-wgted}$ is the population weighted concentration for race k. $C_{i,j}$ is the average pollutant concentration at grid location (i,j). $P^{k}_{i,j}$ is the population data at grid location (i,j) for race k. $(imax,jmax)$ is the maxi-

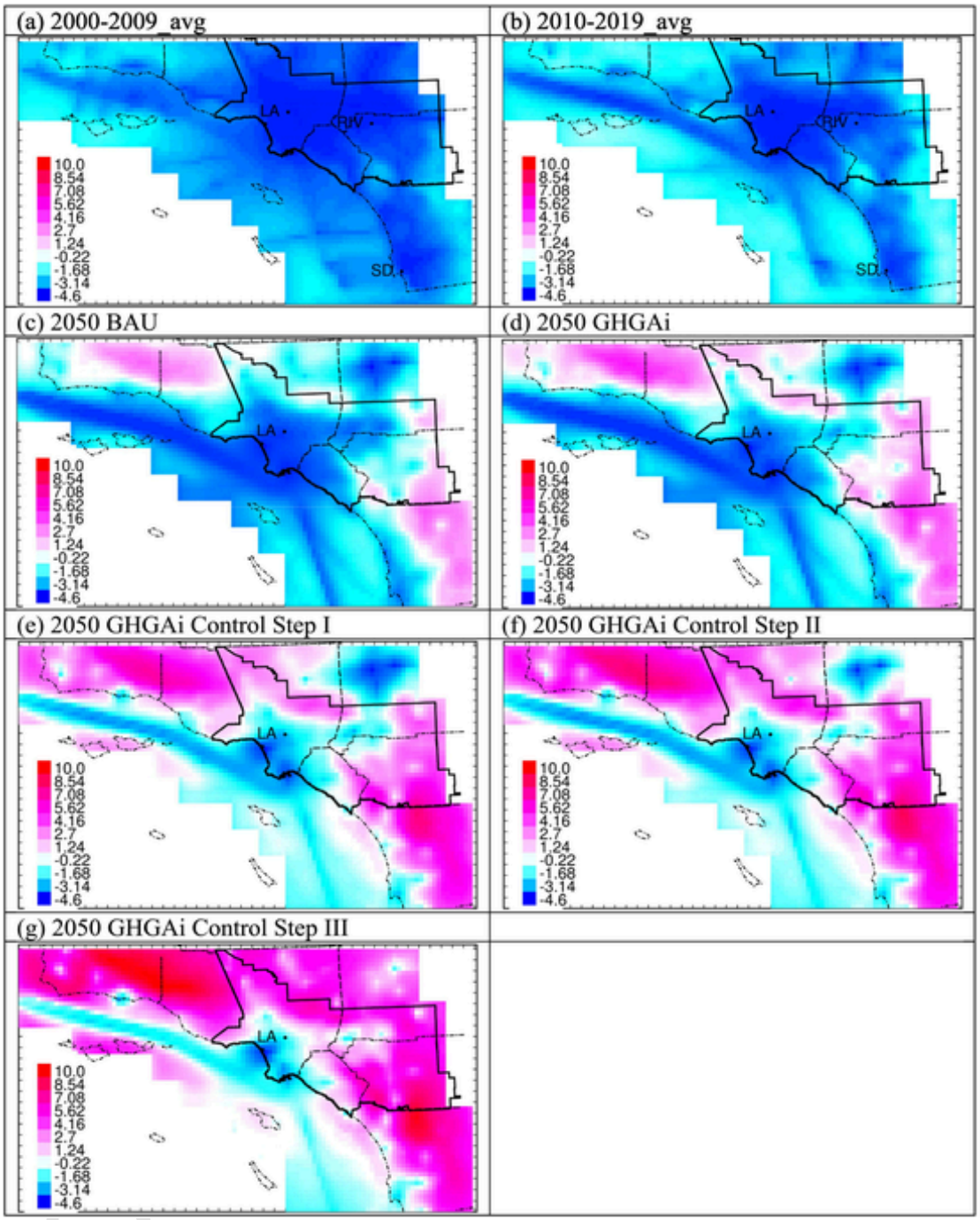

Fig. 4. Formaldehyde to NO_2 (FNR) ratio at hour 13 averaged across 2000–2009, 2010–2019, and the future 32-week simulation period under RCP8.5. Transition value of 4.6 is subtracted from all values. Blue indicates VOC-limited, red indicates NOx-limited.

mum value for grid location (i, j). Based on historical simulations conducted for the 10-year window between 2010 and 2019, the uncertainty (Table S4) in predicted population-weighted concentrations of O_3 and NO_2 associated with the 32-week simulation strategy in Los Angeles would be ± 1.8 ppb and $\pm$ 0.71 ppb, respectively. As discussed below, the actual uncertainty in the disparity calculations is even smaller than this value.

Once population-weighted concentrations were tabulated, the relative environmental disparity for each race/ethnicity group was then calculated as:

$$RD^k = \frac{C^k_{pop-wgted} - C^{All}_{pop-wgted}}{C^{All}_{pop-wgted}} \times 100\%$$

where: RD^k is the relative disparity for race k. $C^k_{pop-wgted}$ is the population weighted concentration for race k. $C^{All}_{pop-wgted}$ is the population weighted concentration for all race/ethnicity groups combined. The uncertainty introduced by the 32-week simulation strategy in Los Angeles is minor because all race/ethnicity groups are affected approximately equally by the meteorological variability that affects total population

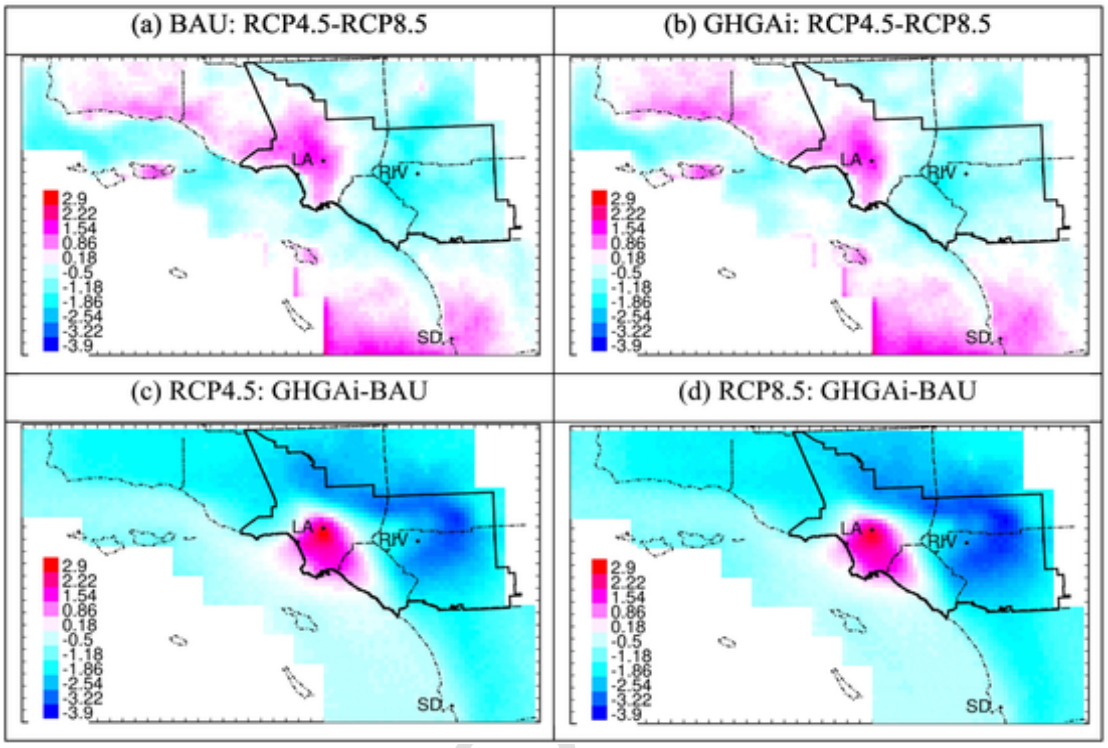

Fig. 5. Impacts of meteorological and emissions changes on 32-week averaged MD8H O_3 under RCP4.5 and RCP8.5 with BAU and GHGAi emission scenarios.

exposures. The maximum exposure disparities associated with the 32-week simulation approach for O_3 and NO_2 are estimated to have an uncertainty of 0.11 ppb and 0.12 ppb, respectively, based on historical simulations between 2010 and 2019 over Los Angeles.

2.3. Threshold for healthy air

In addition to the environmental disparities, we also analyzed the percentage of people living in each study area that experienced unhealthy O_3 or NO_2 concentrations. The O_3 health threshold was set to 35 ppb based on a statistical analysis for respiratory mortality ($P = 0.002$) and circulatory mortality ($P = 0.07$) (Turner et al., 2016). The NO_2 health threshold was set to 4.6 ppb as suggested by the latest World Health Organization (WHO) global air quality guidelines (AQG) (World Health Organization, 2021). The AQG level is the long-term concentration of the pollutant that will generate minimal relevant health outcome. The WHO determined the lowest level of exposure based on the 5th percentile of the exposure distribution from previous studies. The average of the five lowest 5th percentile levels were used as the NO_2 AQG level (8.8 μg/m^3 = 4.6 ppb for NO_2 at 1 atm and 273.15 K).

The percentage of people experiencing unhealthy air quality was calculated as the number of people exposed to O_3 or NO_2 concentrations above the healthy limit divided by the total number of people in the study region.

2.4. Additional experiments to reduce disparity

Residual O_3 and NO_2 exposure disparities under the three GHGAi + control scenarios will be further explored using "brute force" reductions targeted at dominant sources upwind of the affected populations. During this process, the feasibility of the "brute force" reductions will not be discussed, as the main purpose is to verify the effectiveness of the O_3 source apportionment tool for disparity reduction.

3. Results and discussion

3.1. Model performance for 2000–2009 and 2010–2019 periods

The performance of the WRF model for temperature, wind, and relative humidity (Table S5) is consistent with a previous long-term air pollution modeling study in California (Hu et al., 2014). Mean fractional bias (MFB) of temperature and wind are generally within ±0.15. root mean square errors (RMSE) of temperature are generally lower than 4 °C, and RMSE of wind are generally lower than 2 m/s. Table 2 summarizes the CTM performance statistics for MD8H O_3 predictions at four selected urban EPA monitoring sites in Fig. S1 with continuous data for 2000–2009 and 2010–2019 periods. Figs. S5 and S6 show the time series of simulated and observed MD8H O_3 at these monitoring sites for 2000–2009 and 2010–2019 periods. Recommended benchmarks for air quality model performance statistics of MD8H O_3 were taken from Emery et al. (2017). The performance statistics "goals" are Normalized Mean Bias (NMB) < ±5 %, Normalized Mean Error (NME) < 15 %, and Correlation Coefficient (r) > 0.75, which should be viewed as the best a CTM can be expected to achieve. The performance statistics "criteria" are NMB < ±15 %, NME < 25 %, $r > 0.50$, which should be viewed as the skill that most CTMs routinely achieve. The formulas of these performance statistics are provided in Table S4. Of the 24 performance statistics, 10 meet the most stringent "goals" and 13 meet the "criteria". The only performance statistic that slightly exceeds the criteria is the NME value at Los Angeles during the 2000–2009 period. Sharp spatial gradients around the Los Angeles monitoring site associated with fresh NOx emissions may not be fully resolved with the 4 km grid resolution used in the current study. The performance statistics for 2010–2019 are slightly degraded compared to the statistics for 2000–2009, possibly because the lower O_3 concentrations in 2010–2019 could cause larger percentage error even if the value of absolute error didn't change. Note that O_3 concentrations are overestimated in 2013 at Los Angeles and Pasadena due to a wildfire

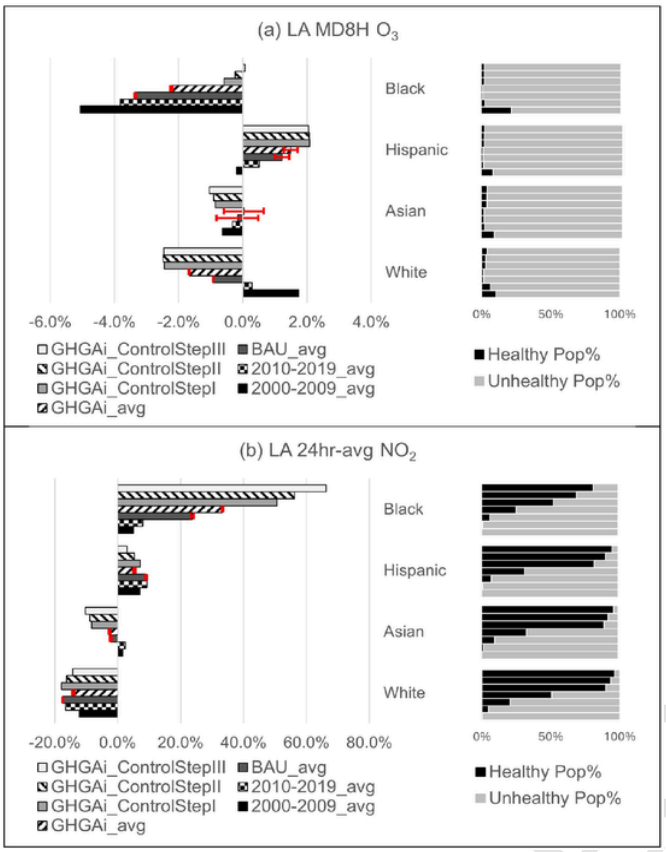

Fig. 6. Relative disparity of population weighted averaged MD8H O_3 and 24hr-avg NO_2 exposure (left) and percentage of population exposed to healthy/unhealthy concentration levels (right) for different race/ethnicity groups at LA. The red error bars of the BAU_avg and GHGAi_avg indicate the disparities under RCP8.5 and RCP4.5 scenarios.

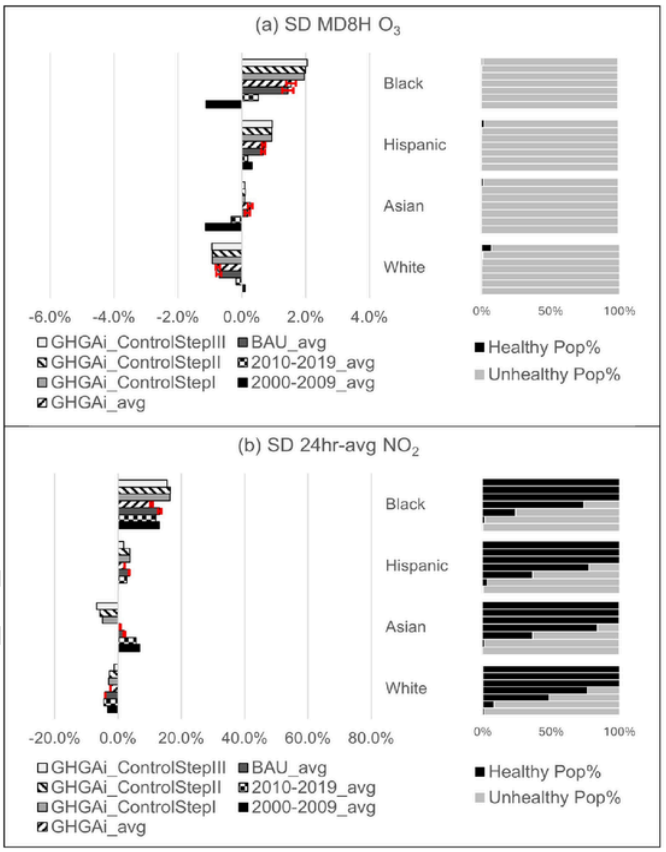

Fig. 7. Relative disparity of population weighted averaged MD8H O_3 and 24hr-avg NO_2 exposure (left) and percentage of population exposed to healthy/unhealthy concentration levels (right) for different race/ethnicity groups at SD. The red error bars of the BAU_avg and GHGAi_avg indicate the disparities under RCP8.5 and RCP4.5 scenarios.

event near the two sites. The model calculations might not accurately represent the details of the wildfire plume dynamics or the microscale meteorology during this isolated event, resulting in an overestimation of O_3 concentrations. However, future simulations will not include random and unpredictable wildfire events and so this issue will not influence calculated exposure disparities. Overall, the performance statistics indicate that simulated O_3 concentrations over the historical time period 2000–2019 are accurate, increasing confidence in the future predictions.

NO_2 predictions are in good agreement with observations for the time period 2000–2009 (Fig. S7) and 2010–2019 (Fig. S8) with both average values and seasonal trends captured. VOC predictions and measurements for formaldehyde, isoprene, benzene, and toluene in Los Angeles for 2000–2019 (Figs. S9 and S10) also have similar average values and seasonal trends, but VOC measurements have greater variability about the averaged concentrations than model predictions, suggesting that VOC emissions inventories do not fully capture the short-term variability of sources. This issue will not affect calculated exposure disparity for NO_2 and O_3. Further details of the VOC comparison are discussed in SI.

3.2. Averaged air quality exposure

Figs. 2 and 3 show the MD8H O_3 and 24 h-avg NO_2 concentrations in Southern California averaged across 2000–2009, 2010–2019, and the 32-week simulation period in 2046–2054 under different future RCP8.5 GHG emission scenarios. MD8H O_3 concentrations significantly

Table 3
Maximum relative disparity differences of MD8H O_3 and 24hr-avg NO_2 exposure between race/ethnicity groups that have highest and lowest exposure under RCP8.5 and RCP4.5 with BAU and GHGAi emission scenarios.

Pollutants	Emission scenario	Max disparity difference under RCP8.5	Max disparity difference under RCP4.5	Change from RCP8.5 to RCP4.5
LA O_3	BAU	4.8 %	4.4 %	−0.4 %
	GHGAi	3.9 %	3.5 %	−0.4 %
LA NO_2	BAU	40.7 %	41.6 %	−0.9 %
	GHGAi	47.7 %	47.2 %	0.5 %
SD O_3	BAU	1.9 %	2.4 %	0.5 %
	GHGAi	2.1 %	2.5 %	0.4 %
SD NO_2	BAU	16.7 %	17.7 %	1.0 %
	GHGAi	12.7 %	13.5 %	0.9 %

Note: $Change\ from\ RCP8.5\ to\ RCP4.5 = Max\ Difference_{RCP4.5} - Max\ Difference_{RCP8.5.}$

increase in the BAU scenario compared to 2000–2009_avg and 2010–2019_avg, while 24 h-avg NO_2 concentrations significantly decrease. For the five future scenarios, both MD8H O_3 and 24 h-avg NO_2 concentrations are significantly reduced in the three increasingly stringent control strategies. The three GHGAi control steps reduced MD8H O_3 concentrations by as much as 8.6 ppb to 12.6 ppb and 24 h-avg NO_2 concentrations by as much as 13.94 ppb to 35.54 ppb compared to the GHGAi scenario (Figs. S11 and S12). Table S6 shows the population weighted O_3 concentration decreases by 9–15 % in LA and

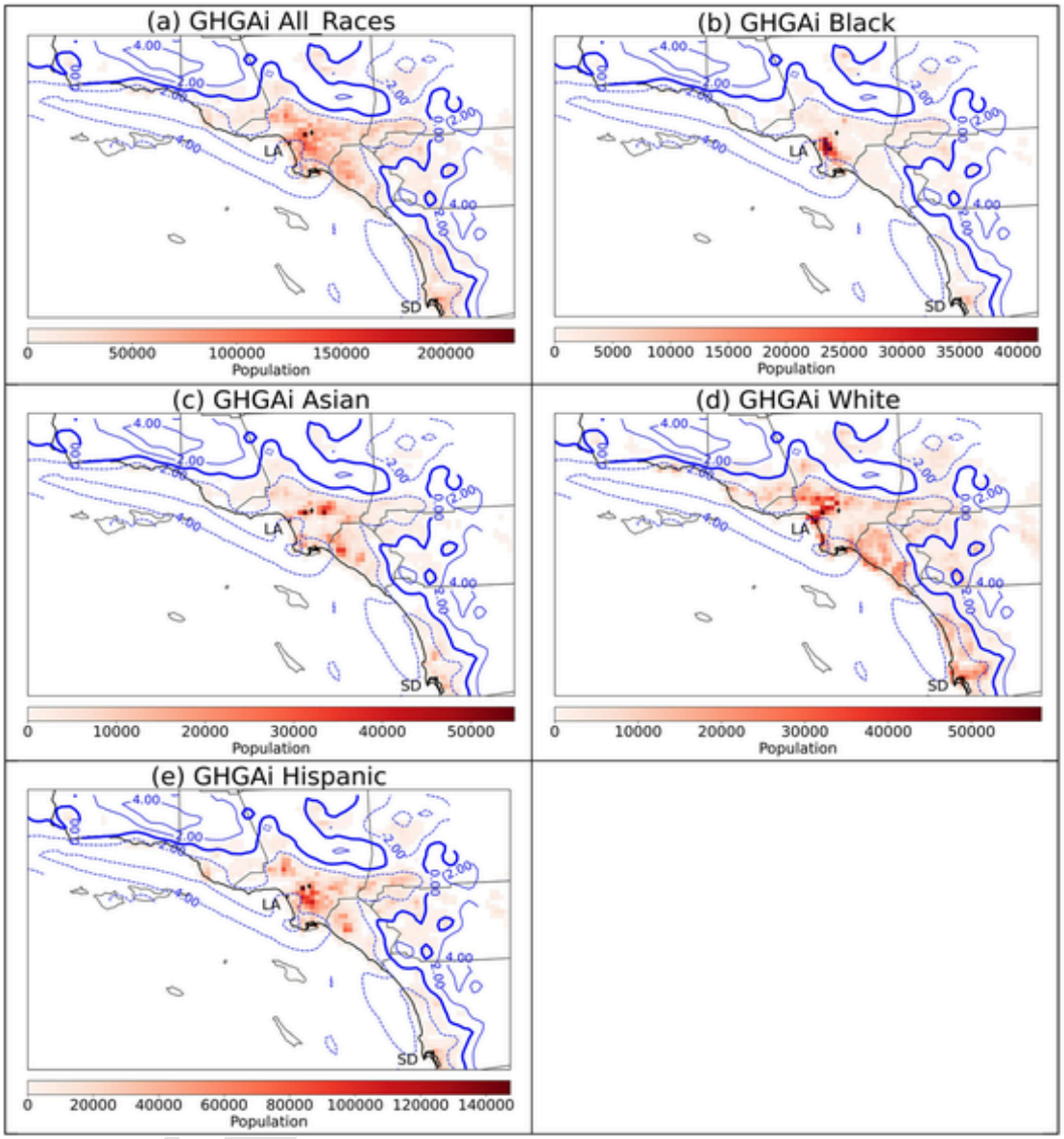

Fig. 8. Population map for different race/ethnicity groups with chemical regimes indicated by FNR under the RCP8.5 GHGAi scenario (blue contour lines are the values of FNR-4.6). Bold contour line indicates transition from NOx-limited chemistry (solid contour lines) to VOC-limited chemistry (dashed contour lines).

12–15 % in SD under the GHGAi scenario. The population weighted NO_2 decreases by >50 % in both LA and SD regions in three supplemental GHGAi control steps. Averaged MD8H O_3 concentrations mainly peak in the north and east portions of SoCAB outside the urban core (Fig. 2). NO_2 concentrations are elevated across the central SoCAB region compared to the outlying regions in 2000–2009 and 2010–2019, but concentrations decrease for future scenarios, with urban hotspots remaining at the port of Long Beach, port of Los Angeles, and Los Angeles International Airport (LAX) (Fig. 3).

Fig. 4 shows the hour 13 Pacific Time HCHO / NO_2 ratio (FNR), corresponding to the typical peak in O_3 concentrations, averaged over 2000–2009, 2010–2019, and the future 32-week simulation periods under a range of RCP8.5 emissions scenarios. The hour 13 FNR value was also used to determine the transition between NOx-limited and VOC-limited chemical regimes in California (Wu et al., 2022). A transition value of 4.6 has been subtracted from the FNR values and the color key has been adjusted so that VOC-limited regions are blue, NOx-limited regions are red, and regions in the transition zone between NOx-limited and VOC-limited chemistry are in white. Both 2000–2009_avg and 2010–2019_avg are VOC-limited across the entire SoCAB. NOx-limited regions start to appear outside the major urban area in the future emissions scenarios as NOx emissions are reduced. The VOC-limited regions in the future scenarios shrink significantly as increasingly stringent emissions controls are applied, but the region between downtown LA and the Port of LA remains VOC-limited under all future emission scenarios.

Fig. S13 shows the population weighted MD8H O_3, 24 h-avg NO_2 concentrations, and the hour 13 FNR values in LA and SD. Population weighted MD8H O_3 in LA and SD increases 7–11 ppb (~16–27 %) in RCP8.5 BAU and RCP8.5 GHGAi scenarios compared to the 2000–2009_avg and 2010–2019_avg period. MD8H O_3 is reduced by <8 ppb (~15 %) compared to the GHGAi concentrations in the three future supplemental control scenarios under RCP8.5. The population weighted 24 h-avg NO_2 concentrations in LA are reduced from 29.1 ppb in 2000–2009_avg to 10.2 ppb under RCP8.5 BAU, and then to 1.93 ppb under the GHGAi_ControlStepIII scenario. The population

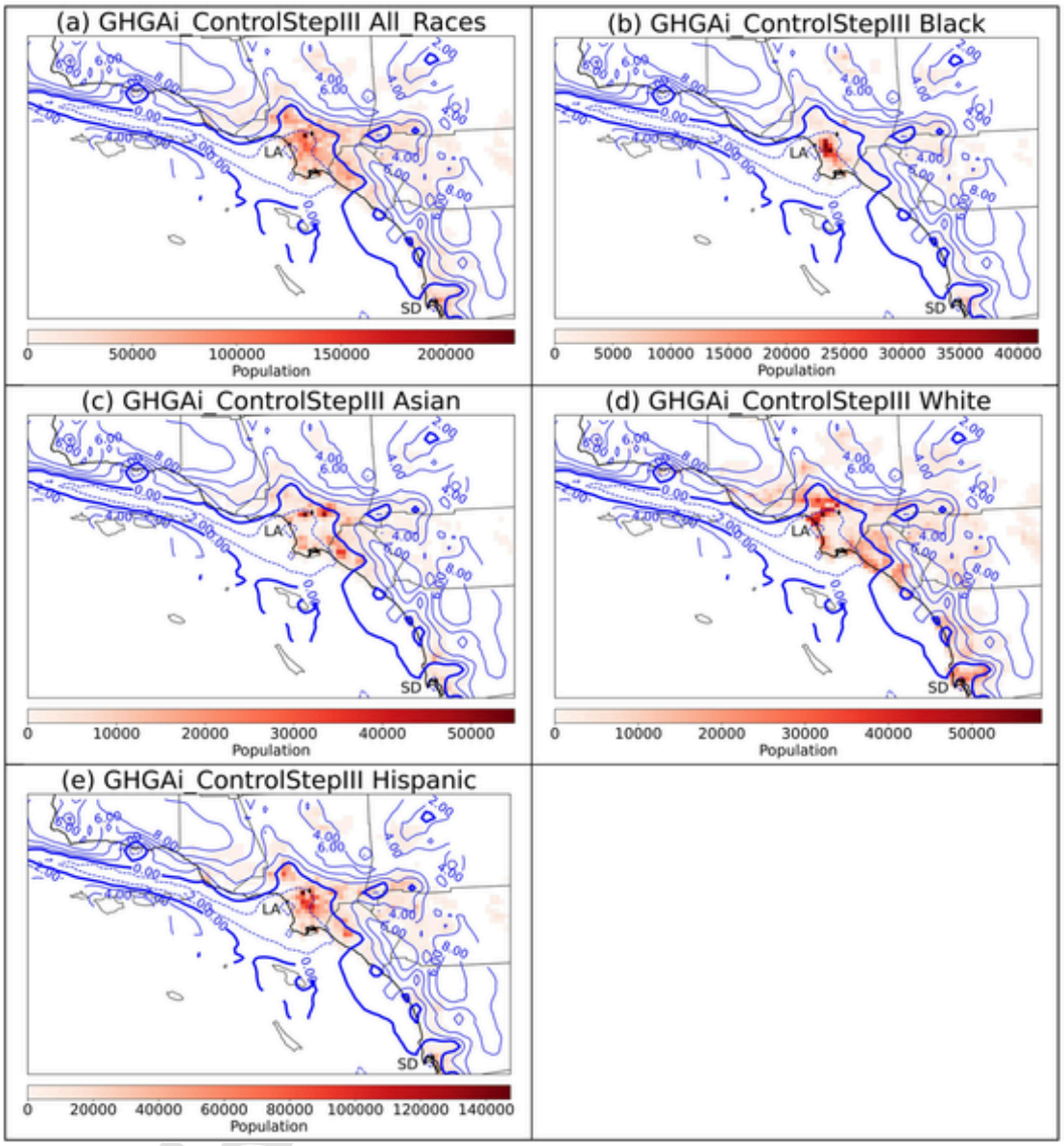

Fig. 9. Population map for different race/ethnicity groups with chemical regimes indicated by FNR under the RCP8.5 GHGAi Control Step III scenario (blue contour lines are the values of FNR-4.6). Bold contour line indicates transition from NOx-limited chemistry (solid contour lines) to VOC-limited chemistry (dashed contour lines).

weighted 24 h-avg NO_2 concentrations in SD are reduced from 16.6 ppb in 2000–2009_avg to 5.0 ppb under RCP8.5 BAU, and then to 1.6 ppb under the GHGAi_ControlStepIII scenario. The population weighted FNR values increase, and the chemical regimes become less VOC-limited as the emissions are reduced. However, using a transition FNR of 4.6, the average resident in the LA and SD regions still lives in the VOC-limited chemical regime under all scenarios analyzed in the current study.

Since O_3 concentrations may also be affected by different climate conditions, we compare the MD8H O_3 changes associated with meteorological conditions under constant emissions to MD8H O_3 changes associated with changing emissions under constant meteorological conditions (Fig. 5). Under the same emission condition, changing from RCP8.5 to RCP4.5 results in MD8H O_3 changes from −2.2 ppb to +2.1 ppb (Fig. 5a and b). Under the same meteorological conditions, changing from BAU to GHGAi emissions results in MD8H O_3 changes from −3.9 ppb to +2.9 ppb (Fig. 5c and b). Thus, emission changes have an equal or greater impact on ozone concentrations than meteorological changes in Southern California. These results are in agreement with the findings from previous studies that also showed that changes in anthropogenic emissions have greater effect on ozone than climate change (Moghani and Archer, 2020; Steiner et al., 2006; Stowell et al., 2017; Tagaris et al., 2007; Wu et al., 2008).

The relative importance of emissions vs. meteorology depends on the analysis time period, since emissions are in continual decline over time whereas climate change strengthens over time. The current study focuses on the mid-century time period when meteorological conditions under different climate scenarios are still somewhat similar to each other. In our simulations, the 32-week average temperatures increase by 0.5–1.1 °C across California from RCP4.5 to RCP8.5. It has been reported that the projected global mean surface air temperature for the mid-21st century would only increase by 1.0–2.0 °C in average from RCP2.6 to RCP8.5 (IPCC, 2013), which is consistent with our simulations. Therefore, we would expect small perturbations in O_3 concentra-

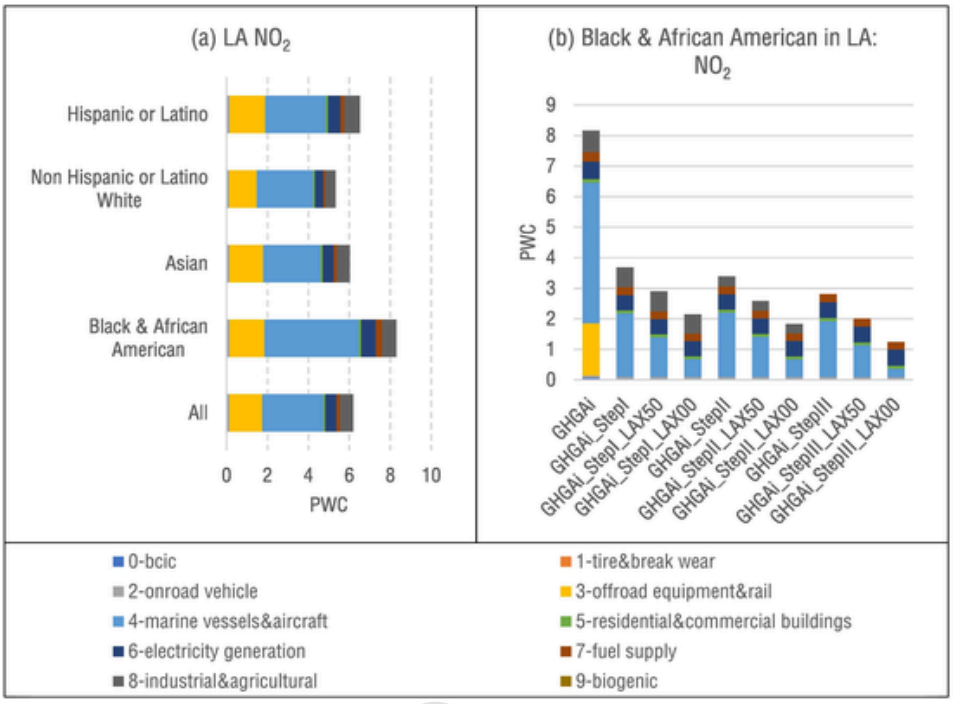

Fig. 10. Population weighted concentrations (PWC) of summertime NO_2 from NOx source apportionment in LA for (a) different race/ethnicity groups under RCP8.5 GHGAi and (b) Black & African Americans under different RCP8.5 scenarios (unit: ppb). BCIC refers to boundary and initial conditions.

tions within such small temperature variations in the near future. Meanwhile, predicted reductions in anthropogenic emissions are big enough to surpass the effects of climate change. A similar analysis conducted in the year 2100 would likely show that meteorological conditions under diverging climate pathways will more significantly influence O_3 concentrations, but this analysis is beyond the scope of the current study.

3.3. Environmental disparities

Tables S7 and S8 tabulate the calculated population weighted O_3 and NO_2 concentrations and their std_devs for difference race/ethnicity groups under different scenarios. The BAU_avg indicates the average of BAU scenarios under RCP8.5 and RCP4.5, and the GHGAi_avg indicates the average of GHGAi scenarios under RCP8.5 and RCP4.5. The std_devs of future scenarios are comparable to the std_devs of 2000–2009_avg and 2010–2019_avg, with std_devs decreasing with increasingly strict emissions controls. Figs. 6a and 7a show the relative exposure disparity of MD8H O_3 (left) and the percentage of population that is exposed to healthy/unhealthy levels of O_3 concentrations (right) in the LA and SD regions averaged for different scenarios. Positive disparity values indicate that the race/ethnicity group is exposed to O_3 concentrations above the population average, while negative disparity values indicate that the group is exposed to O_3 concentrations below the population average. Fig. 6a shows that Hispanic or Latino residents in Los Angeles are exposed to above-average O_3 concentrations under all scenarios except 2000–2009_avg (−0.2 %), with exposure disparities ranging from 0.5 % in 2010–2019_avg to 2.0 % under the GHGAi_ControlStepIII. Black and African American residents experience the lowest O_3 concentrations in 2000–2009_avg, 2010–2019_avg, and the BAU_avg scenario, with exposures of 5.1 %, 3.8 %, and 3.4 % below the average, respectively. However, the absolute O_3 exposure disparity for Black residents decreases under the control scenarios, falling to 2.2 % below the average under GHGAi_avg and to 0.1 % above the average under GHGAi_ControlStepIII. Asian residents in Los Angeles consistently have absolute O_3 exposure disparities within 1 % of the population average across all scenarios. White residents are exposed to higher-than-average O_3 concentrations in 2000–2009_avg and 2010–2019_avg scenarios, with disparities of 1.7 % and 0.3 %, respectively. However, White residents are exposed to lower-than-average O_3 concentrations under all future scenarios, with a maximum disparity of −2.5 % under the strictest emissions controls. In 2000–2009_avg, 21.6 % of Black residents in LA are exposed to MD8H O_3 below 35 ppb, while the ratios for other race/ethnicity groups are approximately 10 %. In 2010–2019_avg, 6.4 % of White residents in LA live in areas with MD8H O_3 below 35 ppb, while the ratios for other race/ethnicity groups are approximately 2 %. Under all future scenarios, <5 % of residents in LA from each race/ethnicity group are exposed to MD8H O_3 below 35 ppb.

O_3 exposure disparities are generally smaller in SD compared to LA (Fig. 7a vs. Fig. 6a). Black residents in San Diego are exposed to below-average O_3 concentrations in 2000–2009_avg, but above-average O_3 concentrations in other scenarios. The Black residents always experience the highest absolute exposure disparities under all scenarios, from 0.5 % to 2.1 %. Hispanic residents are always exposed to above-average O_3 concentrations. Hispanic residents have the highest O_3 exposure in 2000–2009, but second highest O_3 exposure with disparities ranging from 0.6 % to 1.0 % in other scenarios. Asian residents are exposed to below-average O_3 concentrations in 2000–2009_avg and 2010–2019_avg, but above-average O_3 concentrations in all future scenarios. Asian residents have the same exposure disparity as Black residents in 2000–2009_avg (−1.1 %), but very little O_3 exposure disparity in other scenarios. White residents are exposed to slightly above-average O_3 concentrations in 2000–2009_avg with disparity of 0.1 %, but below-average O_3 concentrations in other scenarios with disparities ranging from −0.6 % to −0.9 % as emissions are reduced under different scenarios. None of the residents of different race/ethnicity groups in SD are exposed to MD8H O_3 below 35 ppb in 2000–2009_avg, 2010–2019_avg, BAU_avg or GHGAi_avg. Under the

Table 4
Additional future emission scenarios for exposure disparity reduction.

Scenario	Description
GHGAi_ControlStepI_LAX50	An emission reduction scenario based on GHGAi_ControlStepI scenario that further reduced 50 % NOx emissions from LAX airport
GHGAi_ControlStepII_LAX50	An emission reduction scenario based on GHGAi_ControlStepII scenario that further reduced 50 % NOx emissions from LAX airport
GHGAi_ControlStepIII_LAX50	An emission reduction scenario based on GHGAi_ControlStepIII scenario that further reduced 50 % NOx emissions from LAX airport
GHGAi_ControlStepI_LAX00	An aggressive emission reduction scenario based on GHGAi_ControlStepI scenario that further reduced 100 % NOx emissions from LAX airport
GHGAi_ControlStepII_LAX00	An aggressive emission reduction scenario based on GHGAi_ControlStepII scenario that further reduced 100 % NOx emissions from LAX airport
GHGAi_ControlStepIII_LAX00	An aggressive emission reduction scenario based on GHGAi_ControlStepIII scenario that further reduced 100 % NOx emissions from LAX airport

three GHGAi control scenarios, the percentage of residents exposed to low O_3 concentrations increase from <1 % to 7 %.

Figs. 6b and 7b show the 24 h-avg NO_2 exposure disparity (left) and the percentage of population that is exposed to healthy/unhealthy levels of NO_2 concentrations (right) in the LA and SD regions averaged for different scenarios. In both LA and SD regions, Black and Hispanic residents are consistently exposed to above-average NO_2 concentrations, while White residents are consistently exposed to below-average NO_2 concentrations. Asian residents are exposed to above-average NO_2 concentrations in 2000–2009_avg and 2010–2019_avg, and below-average NO_2 concentrations in the future GHGAi control scenarios in both LA and SD. For BAU_avg and GHGAi_avg scenarios, the 24 h-avg NO_2 concentrations for Asian residents are slightly below the average in LA but slightly above the average in SD.

In the LA region, the relative exposure disparities for Black residents increase significantly as the future control strategies to achieve regulatory compliance reduce emissions from off-road sources in outlying areas. The traditional approach that targets the precursors contributing to the highest regional O_3 concentrations are not optimal for reducing exposure disparities. The traditional control measures reduce NO_2 concentrations more slowly for Black residents compared to the regional average reduction. In both LA and SD, the percentages of Black residents exposed to unhealthy 24 h-avg NO_2 concentrations above 4.6 ppb under all scenarios are always highest, followed by Hispanic, Asian, and then White residents. In SD, all the residents are exposed to NO_2 concentrations below 4.6 ppb under the three future traditional control scenarios, indicating that any residual NO_2 exposure disparity will not affect public health.

In both Figs. 6 and 7, the relative disparities under the RCP4.5 BAU and RCP4.5 GHGAi scenarios are very similar to the RCP8.5 BAU and RCP8.5 GHGAi scenarios, respectively. Using the difference between the RCP4.5 and RCP8.5 results, the uncertainties of relative exposure disparities of MD8H O_3 range from 0.03 % to 0.17 % for Black, 0.05 % to 0.22 % for Hispanic, 0.07 % to 0.65 % for Asian, and 0.0003 % to 0.08 % for White. The uncertainties of relative exposure disparities of 24 h-avg NO_2 range from 0.17 % to 0.53 % for Black, 0.08 % to 0.40 % for Hispanic, 0.21 % to 0.34 % for Asian, and 0.003 % to 0.41 % for White. All the uncertainties of the relative disparities are <0.7 %. The fractional error for the relative disposure disparities (length of the error bar from the center divided by the absolute mean relative disparity) for the highest exposed groups is <18 % for MD8H O_3 and 15 % for 24 h-avg NO_2. Note that fractional errors cannot be calculated for groups with extremely low (~0) exposure disparities.

Table 3 shows the maximum relative disparity differences between race/ethnicity groups that have highest and lowest exposure under RCP8.5 and RCP4.5 with BAU and GHGAi emission scenarios. The changes from RCP8.5 to RCP4.5 range from −0.5 % to 1.0 %, which are relatively small. Overall, the largest relative exposure disparities are not sensitive to the choice of RCP8.5 vs. RCP4.5 climate scenarios.

Figs. 8, 9 and S14–S16 illustrate the population maps for different race/ethnicity groups in Southern California overlaid on contour lines for O_3 formation chemical regimes under different future RCP8.5 scenarios. These maps show that Black residents are clustered in urban core regions with lower FNR regions (NOx-rich), while the other race/ethnicity groups live in outlying regions with higher FNR due to lower NOx concentrations. These spatial patterns explain why NOx emissions reductions have different effects on different race/ethnicity groups. Under the RCP8.5 GHGAi scenario, all race/ethnicity groups live in a NOx-rich atmosphere (Fig. 8). Under the RCP8.5 GHGAi_ControlStepIII scenario, some fraction of the Hispanic, Asian, and White residents transition to a NOx-limited chemical regime, but the Black residents living between central LA and Long Beach remain in a NOx-rich region (Fig. 9). Fig. S17 shows the population weighted FNR centered on 4.6 for different race/ethnicity groups in the LA and SD regions. All race/ethnicity groups live in VOC-limited regions on average under all control scenarios, with the exception that Asian residents live in NOx-limited regions on average under the RCP8.5 GHGAi_ControlStepIII scenario. Black and African American residents always live in the most VOC-limited regions under all control scenarios. Fig. S18 shows the relative disparity of FNR at hour 13 in the LA and SD regions. Black and African American residents are always exposed to below-average FNR values in both LA and SD under all scenarios.

3.4. Disparity reduction strategies for future scenarios

In order to reduce the exposure disparities for Black residents under future scenarios, future sources that contribute to 24 h-avg NO_2 and MD8H O_3 across different race/ethnicity groups were analyzed (Figs. 10 and S19). Figs. 10a and S19a illustrate the NOx source apportionment results of population weighted 24 h-avg NO_2 and MD8H O_3 for different race/ethnicity groups in LA under the RCP8.5 GHGAi scenario. Source contributions to MD8H O_3 are similar across race/ethnicity groups (Fig. S19), while marine vessel and aircraft contributions to 24 h-avg NO_2 are elevated for Black and African American residents in LA (Fig. 10a). Boundary and initial conditions (BCICs) contribute more strongly to O_3 in the control scenarios in both LA and SD but background O_3 is not a dominant source of O_3 exposure disparity. BCICs remain unchanged as emissions are reduced and less background O_3 reacts with local-emitted NOx, causing BCICs to contribute more to relative and absolute concentrations of the residual air pollution in these cleaner scenarios. Biogenic NO emissions in the LA and SD regions are very low relative to anthropogenic NO emissions. Biogenic sources therefore show little to no contributions to NO_2 concentrations in Figs. 10 and S19. Biogenic VOC emissions do contribute significantly to O_3 formation in Southern California (Zhao et al., 2024).

Figs. 10b and S19b show evolving source contributions to 24 h-avg NO_2 and MD8H O_3 for Black & African American residents under future traditional emissions control scenarios. Marine vessels & aircraft remain as significant sources of NO_2 for Black and African American residents under all control scenarios. Considering that 80–90 % of NOx emissions from marine vessels have been reduced, the majority of the remaining emissions are released by aircraft. As Los Angeles International Airport (LAX) is the largest airport in the LA region, two additional disparity reduction scenarios/sensitivity tests with brute-force method were analyzed to explore the effects of reducing local emissions from LAX under each traditional control step. One sensitivity test reduced LAX emissions by 50 % (LAX50) while the second sensitivity test reduced LAX emissions by 100 % (LAX00) under GHGAi StepI, StepII, and StepIII (six additional sensitivity test scenarios – see Table 4). All the sensitivity tests were performed during summer months

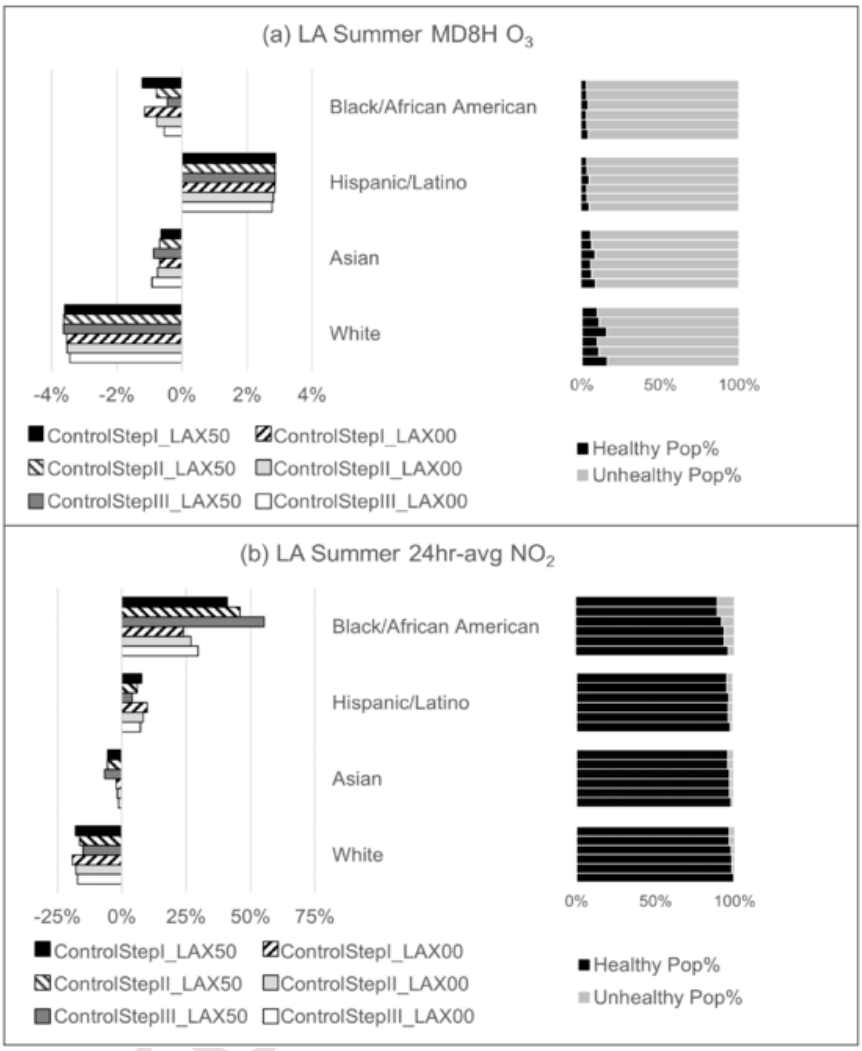

Fig. 11. Relative disparity of population weighted summertime MD8H O_3 and 24hr-avg NO_2 exposure (left) and percentage of population exposed to healthy/unhealthy concentration levels (right) for different race/ethnicity groups under the three control steps with different levels of reduced LAX emissions at LA under RCP8.5.

(June, July & August), when O_3 exceedances are most common (Zhao et al., 2024). The values discussed in the remainder of this analysis all correspond to summer days. Figs. S20 and S21 show the relative disparities for summertime, which have similar patterns as the 32-week average disparity plots. Such similarity also exists for the winter months (December, January & February) (not shown). Therefore, we should expect similar effects of reducing LAX emissions on the relative disparities for summer months to the 32-week average.

Figs. 11, 12, S20 and S21 show the relative disparities for population weighted summertime MD8H O_3 and 24 h-avg NO_2 (left), and percentage of population exposed to healthy/unhealthy concentration levels (right) under the six LAX test scenarios alongside the original control scenarios. Changes to MD8H O_3 exposure disparities for Black and African American residents induced by the additional NOx controls at LAX are minor. However, the relative NO_2 exposure disparities for Black and African American residents in LA are reduced significantly as NOx at LAX is controlled. Reducing LAX emissions by 50 % reduces the NO_2 exposure disparity for Black and African American residents from 53.1 % to 40.9 % for Control Step I, from 59.3 % to 45.8 % for Control Step II, and from 71.3 % to 55.3 % for Control Step III. The total removal of LAX emissions reduces the NO_2 exposure disparity for Black and African American residents from 53.1 % to 23.9 % for Control Step I, 59.3 % to 26.8 % for Control Step II, and 71.3 % to 29.6 % for Control Step III. The percentage of Black and African American residents who are exposed to unhealthy 24 h-avg NO_2 concentrations (≥4.6 ppb) decreases significantly, from >22 % under original control scenarios to <10 % after LAX emissions scenarios are eliminated. Reductions in LAX emissions have minor effect on the NO_2 exposure disparities for other race/ethnicity groups since they are not concentrated in regions immediately downwind of the airport.

It should be noted that all the sensitivity tests for LAX emissions are unrealistic based on current technology. Elimination of NOx emissions from jet aircraft would require new control technology that does not yet exist. The main purpose of the sensitivity analysis conducted here is to verify the source tagging results that identify LAX emissions as a major source of NOx exposure for downwind residents.

4. Conclusion

This study has focused on the future EJ analysis of O_3 and NO_2 exposure disparities under different emissions reduction scenarios. Previous studies show that biogenic VOC emissions would prevent attainment of O_3 standards in Southern California, making NOx control the only viable long-term strategy. While controlling NOx emissions, policy mak-

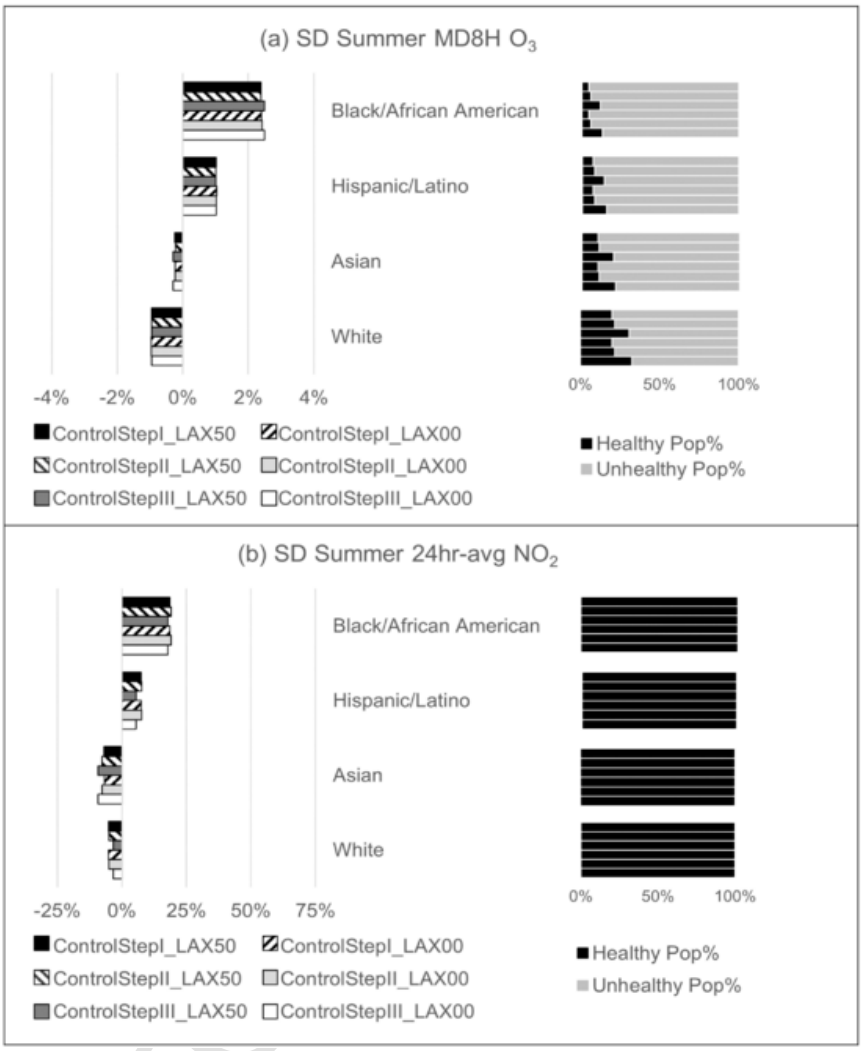

Fig. 12. Relative disparity of population weighted summertime MD8H O_3 and 24hr-avg NO_2 exposure (left) and percentage of population exposed to healthy/unhealthy concentration levels (right) for different race/ethnicity groups under the three control steps with different levels of reduced LAX emissions at SD under RCP8.5.

ers should keep in mind that small reductions in NOx emissions may cause increases in O_3 concentrations, and only a deep cut in NOx emissions can avoid such disbenefits. Future emissions control programs can be developed to reduce O_3 concentrations in Southern California after the adoption of low-carbon energy scenarios through reductions targeting residual sources of precursor NOx emissions. However, these traditional control strategies do not reduce environmental disparities for O_3 and NO_2 across different race and ethnicity groups in the Los Angeles region. Relative exposure disparities of MD8H O_3 and 24 h-avg NO_2 even increase for the Black and African American communities under the future emissions control strategies studied here. Black and African American residents live in the urban core of LA that has higher NOx concentrations compared to outlying regions. Controls targeting NOx sources reduce NOx concentrations for the Black residents, but the O_3 chemistry does not transition fully to NOx-limited conditions in the urban core region, resulting in slower MD8H O_3 reductions for Black residents compared to the general population. Meanwhile, as the absolute 24 h-avg NO_2 concentrations are much lower for the general population than for the Black residents, the relative exposure disparities for Black residents respond more slowly than for other residents. This finding emphasizes the need to consider environmental justice as a main objective when beginning the design of emissions control strategies.

This study demonstrates a novel method to develop controls optimized to reduce exposure disparity, using the source-apportionment capabilities of the CTMs that were used to design emissions controls. Emissions from the Los Angeles International Airport (LAX) were identified as a significant contributor to NO_2 exposure disparities for Black and African American residents in Los Angeles. Sensitivity tests were conducted by reducing the LAX emissions by 50 % and 100 % under each of the three traditional control scenarios to confirm this finding. The sensitivity tests significantly reduced the relative disparities of 24 h-avg NO_2 exposures for Black residents by up to 50 %. The feasibility of reducing emissions from major airports is beyond the scope of the current analysis, but the results demonstrate that the same tools (O_3 source apportionment technique) used to develop control strategies for compliance with regional air pollution regulations can also be used to develop effective control strategies to reduce exposure disparities to photochemical pollutants even in the presence of non-linear chemical reactions that change response factors across regions. Note that the O_3 source apportionment technique can also identify emissions contributions by geographical regions, but these results are not discussed in the current study. Future studies should take advantage of these capabilities to design emissions control programs to reduce exposure disparities.

The choice of background climate scenario did not strongly influence the projected O_3 and NO_2 exposure disparities. Results generated under the RCP4.5 scenario coupled with BAU and GHGAi emission scenarios were similar to the results from the RCP8.5 BAU and GHGAi scenarios. As the future period of this study is 2050, the changes to mean surface air temperature under different climate scenarios are modest, which limits the impact on O_3 concentrations. Studies that look at disparities in the year 2100 will need to more comprehensively consider background climate effects on O_3 concentrations.

The current study considered criteria pollutant emissions reductions across the entire state of California with a focus on impacts in the Southern California region. Changes to criteria pollutant emissions outside of California were not considered. Emissions reductions outside California can affect upwind concentrations of pollutants but these generally have minor influence in Southern California (represented as the BCIC in the current study). Local emissions sources are the dominant factor that affects the exposure disparities in Los Angeles under the BAU and GHGAi scenarios. Assuming that BCICs will not change by an order of magnitude between present day and 2050, the conclusions about the sources of O_3 and NO_2 exposure disparity are not sensitive to the choice of upwind boundary conditions. Simulations conducted further into the future (~year 2100) may need to consider these changes to upwind boundary conditions when calculating contributions to exposure disparities, but this analysis is beyond the scope of the current study.

CRediT authorship contribution statement

Yusheng Zhao: Writing – review & editing, Writing – original draft, Formal analysis. **Yin Li:** Resources, Methodology. **Yiting Li:** Resources, Methodology. **Anikender Kumar:** Resources, Methodology. **Michael J. Kleeman:** Writing – review & editing, Writing – original draft, Supervision, Software, Project administration, Methodology, Funding acquisition, Formal analysis, Conceptualization.

Declaration of competing interest

The authors declare the following financial interests/personal relationships which may be considered as potential competing interests: Michael Kleeman reports financial support was provided by Climateworks Foundation.

Acknowledgements

This study was partially funded by the United States Environmental Protection Agency under Grant No. R83587901. Although the research described in the article has been funded by the United States Environmental Protection Agency it has not been subject to the Agency's required peer and policy review and therefore does not necessarily reflect the reviews of the Agency and no official endorsement should be inferred.

Data availability

Data will be made available on request.

Appendix A. Supplementary data

Supplementary data to this article can be found online at https://doi.org/10.1016/j.scitotenv.2025.178379.

References

Anderson, C.M., Kissel, K.A., Field, C.B., Mach, K.J., 2018. Climate change mitigation, air pollution, and environmental justice in California. Environ. Sci. Technol. 52, 10829–10838. https://doi.org/10.1021/acs.est.8b00908.

Bluhm, R., Polonik, P., Hemes, K.S., Sanford, L.C., Benz, S.A., Levy, M.C., Ricke, K.L., Burney, J.A., 2022. Disparate air pollution reductions during California's COVID-19 economic shutdown. Nat. Sustain. 5, 509–517. https://doi.org/10.1038/s41893-022-00856-1.

Boyce, J.K., Pastor, M., 2013. Clearing the air: incorporating air quality and environmental justice into climate policy. Clim. Change 120, 801–814. https://doi.org/10.1007/s10584-013-0832-2.

Bravo, M.A., Anthopolos, R., Bell, M.L., Miranda, M.L., 2016. Racial isolation and exposure to airborne particulate matter and ozone in understudied US populations: environmental justice applications of downscaled numerical model output. Environ. Int. 92–93, 247–255. https://doi.org/10.1016/j.envint.2016.04.008.

California Air Resources Board, 2006. AB-32 Air pollution: greenhouse gases: California Global Warming Solutions Act of 2006 [WWW Document]. https://leginfo.legislature.ca.gov/faces/billNavClient.xhtml?bill_id=200520060AB32https://leginfo.legislature.ca.gov/faces/billNavClient.xhtml?bill_id=200520060AB32. (accessed 6.28.23).

Carter, W.P.L., Heo, G., 2013. Development of revised SAPRC aromatics mechanisms. Atmos. Environ. 77, 404–414. https://doi.org/10.1016/j.atmosenv.2013.05.021.

Cohan, D.S., Napelenok, S.L., 2011. Air quality response modeling for decision support. Atmosphere (Basel). 2, 407–425. https://doi.org/10.3390/atmos2030407.

Collins, T.W., Grineski, S.E., Nadybal, S.M., 2022. A comparative approach for environmental justice analysis: explaining divergent societal distributions of particulate matter and ozone pollution across U.S. Neighborhoods. Ann. Am. Assoc. Geogr. 112, 522–541. https://doi.org/10.1080/24694452.2021.1935690.

Colmer, J., Hardman, I., Shimshack, J., Voorheis, J., 2020. Disparities in PM 2.5 air pollution in the United States. Science (80-.) 369, 575–578. https://doi.org/10.1126/science.aaz9353.

Cushing, L., Faust, J., August, L.M., Cendak, R., Wieland, W., Alexeeff, G., 2015. Racial/ethnic disparities in cumulative environmental health impacts in California: evidence from a statewide environmental justice screening tool (CalEnviroScreen 1.1). Am. J. Public Health 105, 2341–2348. https://doi.org/10.2105/AJPH.2015.302643.

Do, K., Yu, H., Velasquez, J., Grell-Brisk, M., Smith, H., Ivey, C.E., 2021. A data-driven approach for characterizing community scale air pollution exposure disparities in inland Southern California. J. Aerosol Sci. 152, 105704. https://doi.org/10.1016/j.jaerosci.2020.105704.

Emery, C., Liu, Z., Russell, A.G., Odman, M.T., Yarwood, G., Kumar, N., 2017. Recommendations on statistics and benchmarks to assess photochemical model performance. J. Air Waste Manag. Assoc. 67, 582–598. https://doi.org/10.1080/10962247.2016.1265027.

Gallagher, C.L., Holloway, T., 2022. U.S. decarbonization impacts on air quality and environmental justice. Environ. Res. Lett. 17. https://doi.org/10.1088/1748-9326/ac99ef.

Goodkind, A.L., Tessum, C.W., Coggins, J.S., Hill, J.D., Marshall, J.D., 2019. Fine-scale damage estimates of particulate matter air pollution reveal opportunities for location-specific mitigation of emissions. Proc. Natl. Acad. Sci. 116, 8775–8780. https://doi.org/10.1073/pnas.1816102116.

Houston, D., Wu, J., Ong, P., Winer, A., 2004. Structural disparities of urban traffic in Southern California: implications for vehicle-related air pollution exposure in minority and high-poverty neighborhoods. J. Urban Aff. 26, 565–592. https://doi.org/10.1111/j.0735-2166.2004.00215.x.

Hu, J., Zhang, H., Chen, S.-H., Wiedinmyer, C., Vandenberghe, F., Ying, Q., Kleeman, M.J., 2014. Predicting primary PM 2.5 and PM 0.1 trace composition for epidemiological studies in California. Environ. Sci. Technol. 48, 4971–4979. https://doi.org/10.1021/es404809j.

Hu, J., Zhang, H., Ying, Q., Chen, S.-H., Vandenberghe, F., Kleeman, M.J., 2015. Long-term particulate matter modeling for health effect studies in California – part 1: model performance on temporal and spatial variations. Atmos. Chem. Phys. 15, 3445–3461. https://doi.org/10.5194/acp-15-3445-2015.

IPCC, 2013. Summary for Policymakers, in: Climate Change 2013: The Physical Science Basis. (Contribution of Working Group I to the Fifth Assessment Report of the Intergovernmental Panel on Climate Change).

Kheirbek, I., Wheeler, K., Walters, S., Kass, D., Matte, T., 2013. PM2.5 and ozone health impacts and disparities in New York City: sensitivity to spatial and temporal resolution. Air Qual. Atmos. Heal. 6, 473–486. https://doi.org/10.1007/s11869-012-0185-4.

Lane, H.M., Morello-Frosch, R., Marshall, J.D., Apte, J.S., 2022. Historical redlining is associated with present-day air pollution disparities in U.S. Cities. Environ. Sci. Technol. Lett. 9, 345–350. https://doi.org/10.1021/acs.estlett.1c01012.

Li, Yin, Yang, C., Li, Yiting, Kumar, A., Kleeman, M.J., 2022. Future emissions of particles and gases that cause regional air pollution in California under different greenhouse gas mitigation strategies. Atmos. Environ. 273, 118960. https://doi.org/10.1016/j.atmosenv.2022.118960.

Li, Yiting, Kumar, A., Hamilton, S., Lea, J.D., Harvey, J., Kleeman, M.J., 2022a. Optimized environmental justice calculations for air pollution disparities in Southern California. Heliyon 8, e10732. https://doi.org/10.1016/j.heliyon.2022.e10732.

Li, Yiting, Kumar, A., Li, Yin, Kleeman, M.J., 2022b. Adoption of low-carbon fuels reduces race/ethnicity disparities in air pollution exposure in California. Sci. Total Environ. 834, 155230. https://doi.org/10.1016/j.scitotenv.2022.155230.

Lin, M., Fiore, A.M., Horowitz, L.W., Langford, A.O., Oltmans, S.J., Tarasick, D., Rieder, H.E., 2015. Climate variability modulates western US ozone air quality in spring via deep stratospheric intrusions. Nat. Commun. 6, 1–11. https://doi.org/10.1038/ncomms8105.

Liu, J., Clark, L.P., Bechle, M.J., Hajat, A., Kim, S.Y., Robinson, A.L., Sheppard, L., Szpiro, A.A., Marshall, J.D., 2021. Disparities in air pollution exposure in the United States by race/ethnicity and income, 1990–2010. Environ. Health Perspect. 129, 1–14. https://doi.org/10.1289/EHP8584.

Luo, Q., Copeland, B., Garcia-Menendez, F., Johnson, J.X., 2022. Diverse pathways for power sector Decarbonization in Texas yield health Cobenefits but fail to alleviate air

pollution exposure inequities. Environ. Sci. Technol. 56, 13274–13283. https://doi.org/10.1021/acs.est.2c00881.
Miranda, M.L., Edwards, S.E., Keating, M.H., Paul, C.J., 2011. Making the environmental justice grade: the relative burden of air pollution exposure in the United States. Int. J. Environ. Res. Public Health 8, 1755–1771. https://doi.org/10.3390/ijerph8061755.
Mitchell, G., Dorling, D., 2003. An environmental justice analysis of British air quality. Environ. Plan. A Econ. Sp. 35, 909–929. https://doi.org/10.1068/a35240.
Mitchell, G., Norman, P., Mullin, K., 2015. Who benefits from environmental policy? An environmental justice analysis of air quality change in Britain, 2001–2011. Environ. Res. Lett. 10, 105009. https://doi.org/10.1088/1748-9326/10/10/105009.
Moghani, M., Archer, C.L., 2020. The impact of emissions and climate change on future ozone concentrations in the USA. Air Qual. Atmos. Heal. 13, 1465–1476. https://doi.org/10.1007/s11869-020-00900-z.
Morelli, X., Gabet, S., Rieux, C., Bouscasse, H., Mathy, S., Slama, R., 2019. Which decreases in air pollution should be targeted to bring health and economic benefits and improve environmental justice? Environ. Int. 129, 538–550. https://doi.org/10.1016/j.envint.2019.04.077.
Morello-Frosch, R., Pastor, M., Porras, C., Sadd, J., 2002. Environmental justice and regional inequality in southern California: implications for future research. Environ. Health Perspect. 110, 149–154. https://doi.org/10.1289/ehp.02110s2149.
National Centers for Environmental Prediction, National Weather Service, NOAA, U.S. Department of Commerce, 1980a. NCEP ADP operational global surface observations, February 1975 - February 2007. Res. Data Arch. Natl. Cent. Atmos. Res. Comput. Inf. Syst. Lab. https://doi.org/10.5065/E6NW-HY91.
National Centers for Environmental Prediction, National Weather Service, NOAA, U.S. Department of Commerce, 1980b. NCEP ADP Operational Global Upper Air Observations, December 1972 - February 2007. Res. Data Arch. Natl. Cent. Atmos. Res. Comput. Inf. Syst. Lab. https://doi.org/10.5065/WPBD-ZK78.
National Centers for Environmental Prediction, National Weather Service, NOAA, U.S. Department of Commerce, 2004a. NCEP ADP Global Surface Observational Weather Data, October 1999 - continuing. Res. Data Arch. Natl. Cent. Atmos. Res. Comput. Inf. Syst. Lab. https://doi.org/10.5065/4F4P-E398.
National Centers for Environmental Prediction, National Weather Service, NOAA, U.S. Department of Commerce, 2004b. NCEP ADP global upper air observational weather data, October 1999 - continuing. Res. Data Arch. Natl. Cent. Atmos. Res. Comput. Inf. Syst. Lab. https://doi.org/10.5065/39C5-Z211.
National Centers for Environmental Prediction, National Weather Service, NOAA, U.S. Department of Commerce, 2005. NCEP North American Regional Reanalysis (NARR). Res. Data Arch. Natl. Cent. Atmos. Res. Comput. Inf. Syst, Lab.
Nguyen, N.P., Marshall, J.D., 2018. Impact, efficiency, inequality, and injustice of urban air pollution: variability by emission location. Environ. Res. Lett. 13, 024002. https://doi.org/10.1088/1748-9326/aa9cb5.
Pfannerstill, E.Y., Arata, C., Zhu, Q., Schulze, B.C., Ward, R., Woods, R., Harkins, C., Schwantes, R.H., Seinfeld, J.H., Bucholtz, A., Cohen, R.C., Goldstein, A.H., 2024. Temperature-dependent emissions dominate aerosol and ozone formation in Los Angeles. Science (80-.) 384, 1324–1329. https://doi.org/10.1126/science.adg8204.
Picciano, P., Qiu, M., Eastham, S.D., Yuan, M., Reilly, J., Selin, N.E., 2023. Air quality related equity implications of U.S. decarbonization policy. Nat. Commun. 14, 5543. https://doi.org/10.1038/s41467-023-41131-x.
Pope, R., Wu, J., Boone, C., 2016. Spatial patterns of air pollutants and social groups: a distributive environmental justice study in the phoenix metropolitan region of USA. Environ. Manag. 58, 753–766. https://doi.org/10.1007/s00267-016-0741-z.
Research Data Archive, Computational and Information Systems Laboratory, National Center for Atmospheric Research, University Corporation for Atmospheric Research, and C.C.S.M., Climate and Global Dynamics Division, National Center for Atmospheric Research, University Corporation for Atmospheric Research, 2011. NCAR Community Earth System Model, EaSM Project Dataset. Res. Data Arch. Natl. Cent. Atmos. Res. Comput. Inf. Syst. Lab.
Saha, S., Moorthi, S., Pan, H.-L., Wu, X., Wang, Jiande, Nadiga, S., Tripp, P., Kistler, R., Woollen, J., Behringer, D., Liu, H., Stokes, D., Grumbine, R., Gayno, G., Wang, Jun, Hou, Y.-T., Chuang, H., Juang, H.-M.H., Sela, J., Iredell, M., Treadon, R., Kleist, D., Van Delst, P., Keyser, D., Derber, J., Ek, M., Meng, J., Wei, H., Yang, R., Lord, S., van den Dool, H., Kumar, A., Wang, W., Long, C., Chelliah, M., Xue, Y., Huang, B., Schemm, J.-K., Ebisuzaki, W., Lin, R., Xie, P., Chen, M., Zhou, S., Higgins, W., Zou, C.-Z., Liu, Q., Chen, Y., Han, Y., Cucurull, L., Reynolds, R.W., Rutledge, G., Goldberg, M., 2010. NCEP climate forecast system reanalysis (CFSR) 6-hourly products, January 1979 to December 2010. Res. Data Arch. Natl. Cent. Atmos. Res. Comput. Inf. Syst. Lab. https://doi.org/10.5065/D69K487J.
Saha, S., Moorthi, S., Wu, X., Wang, J., Nadiga, S., Tripp, P., Behringer, D., Hou, Y.-T., Chuang, H., Iredell, M., Ek, M., Meng, J., Yang, R., Mendez, M.P., van den Dool, H., Zhang, Q., Wang, W., Chen, M., Becker, E., 2014. NCEP climate forecast system version 2 (CFSv2) 6-hourly products. Res. Data Arch. Natl. Cent. Atmos. Res. Comput. Inf. Syst. Lab. https://doi.org/10.5065/D61C1TXF.
Schwalm, C.R., Glendon, S., Duffy, P.B., 2020. RCP8.5 tracks cumulative CO2 emissions. Proc. Natl. Acad. Sci. 117, 19656–19657. https://doi.org/10.1073/pnas.2007117117.
Shah, R.U., Robinson, E.S., Gu, P., Apte, J.S., Marshall, J.D., Robinson, A.L., Presto, A.A., 2020. Socio-economic disparities in exposure to urban restaurant emissions are larger than for traffic. Environ. Res. Lett. 15, 114039. https://doi.org/10.1088/1748-9326/abbc92.
Steiner, A.L., Tonse, S., Cohen, R.C., Goldstein, A.H., Harley, R.A., 2006. Influence of future climate and emissions on regional air quality in California. J. Geophys. Res. Atmos. 111. https://doi.org/10.1029/2005JD006935.
Stowell, J.D., Kim, Y. min, Gao, Y., Fu, J.S., Chang, H.H., Liu, Y., 2017. The impact of climate change and emissions control on future ozone levels: implications for human health. Environ. Int. 108, 41–50. https://doi.org/10.1016/j.envint.2017.08.001.
Tagaris, E., Manomaiphiboon, K., Liao, K., Leung, L.R., Woo, J., He, S., Amar, P., Russell, A.G., 2007. Impacts of global climate change and emissions on regional ozone and fine particulate matter concentrations over the United States. J. Geophys. Res. Atmos. 112. https://doi.org/10.1029/2006JD008262.
Tessum, C.W., Hill, J.D., Marshall, J.D., 2017. InMAP: a model for air pollution interventions. PloS One 12, e0176131. https://doi.org/10.1371/journal.pone.0176131.
Tessum, C.W., Paolella, D.A., Chambliss, S.E., Apte, J.S., Hill, J.D., Marshall, J.D., 2021. PM2.5 polluters disproportionately and systemically affect people of color in the United States. Sci. Adv. 7, 1–6. https://doi.org/10.1126/sciadv.abf4491.
Thind, M.P.S., Tessum, C.W., Azevedo, I.L., Marshall, J.D., 2019. Fine particulate air pollution from electricity generation in the US: health impacts by race, income, and geography. Environ. Sci. Technol. 53, 14010–14019. https://doi.org/10.1021/acs.est.9b02527.
Turner, M.C., Jerrett, M., Pope, C.A., Krewski, D., Gapstur, S.M., Diver, W.R., Beckerman, B.S., Marshall, J.D., Su, J., Crouse, D.L., Burnett, R.T., 2016. Long-term ozone exposure and mortality in a large prospective study. Am. J. Respir. Crit. Care Med. 193, 1134–1142. https://doi.org/10.1164/rccm.201508-1633OC.
U.S. Census Bureau, 2020. American community survey (ACS) data [WWW document]. URL https://www2.census.gov/geo/tiger/TIGER_DP/ (accessed 12.14.20).
U.S. Census Bureau, 2021. 2020 Census Redistricting Data (Public Law 94-171) Summary File.
U.S. EPA, 2024a. Our Nation's air trends through 2023 [WWW document]. https://gispub.epa.gov/air/trendsreport/2024.
U.S. EPA, 2024b. Environmental justice: Learn about environmental justice [WWW document]. URL https://www.epa.gov/environmentaljustice/learn-about-environmental-justice (accessed 9.30.24).
Venecek, M.A., Cai, C., Kaduwela, A., Avise, J., Carter, W.P.L., Kleeman, M.J., 2018a. Analysis of SAPRC16 chemical mechanism for ambient simulations. Atmos. Environ. 192, 136–150. https://doi.org/10.1016/j.atmosenv.2018.08.039.
Venecek, M.A., Yu, X., Kleeman, M.J., 2018b. Ultrafine particulate matter source contributions across the continental United States. Atmos. Chem. Phys. Discuss. 1–26. https://doi.org/10.5194/acp-2018-833.
Venecek, M.A., Yu, X., Kleeman, M.J., 2019. Predicted ultrafine particulate matter source contribution across the continental United States during summertime air pollution events. Atmos. Chem. Phys. 19, 9399–9412. https://doi.org/10.5194/acp-19-9399-2019.
Wang, Y., Apte, J.S., Hill, J.D., Ivey, C.E., Patterson, R.F., Robinson, A.L., Tessum, C.W., Marshall, J.D., 2022. Location-specific strategies for eliminating US national racial-ethnic PM2.5 exposure inequality. Proc. Natl. Acad. Sci. U. S. A. 119, 1–7. https://doi.org/10.1073/pnas.2205548119.
Wang, Yifan, Liu, P., Schwartz, J., Castro, E., Wang, W., Chang, H., Scovronick, N., Shi, L., 2023b. Disparities in ambient nitrogen dioxide pollution in the United States. Proc. Natl. Acad. Sci. 120, 2017. https://doi.org/10.1073/pnas.2208450120.
Wang, Yuzhou, Apte, J.S., Hill, J.D., Ivey, C.E., Johnson, D., Min, E., Morello-Frosch, R., Patterson, R., Robinson, A.L., Tessum, C.W., Marshall, J.D., 2023a. Air quality policy should quantify effects on disparities. Science (80-.) 381, 272–274. https://doi.org/10.1126/science.adg9931.
World Health Organization, 2021. WHO global air quality guidelines Particulate matter (PM2.5 and PM10), ozone, nitrogen dioxide, sulfur dioxide and carbon monoxide 1–360.
World Health Organization, 2022. Ambient (outdoor) air pollution [WWW Document]. URL https://www.who.int/news-room/fact-sheets/detail/ambient-(outdoor)-air-quality-and-health
Wu, S., Mickley, L.J., Jacob, D.J., Rind, D., Streets, D.G., 2008. Effects of 2000-2050 changes in climate and emissions on global tropospheric ozone and the policy-relevant background surface ozone in the United States. J. Geophys. Res. Atmos. 113. https://doi.org/10.1029/2007JD009639.
Wu, S., Lee, H.J., Anderson, A., Liu, S., Kuwayama, T., Seinfeld, J.H., Kleeman, M.J., 2022. Direct measurements of ozone response to emissions perturbations in California. Atmos. Chem. Phys. 22, 4929–4949. https://doi.org/10.5194/acp-22-4929-2022.
Wu, S., Alaimo, C.P., Zhao, Y., Green, P.G., Young, T.M., Liu, S., Kuwayama, T., Coggon, M.M., Stockwell, C.E., Xu, L., Warneke, C., Gilman, J.B., Robinson, M.A., Veres, P.R., Neuman, J.A., Kleeman, M.J., 2024. O 3 sensitivity to NO x and VOC during RECAP-CA: implication for emissions control strategies. ACS ES&T Air. https://doi.org/10.1021/acsestair.4c00026.
Xu, L., Yu, J.Y., Schnell, J.L., Prather, M.J., 2017. The seasonality and geographic dependence of ENSO impacts on U.S. surface ozone variability. Geophys. Res. Lett. 44, 3420–3428. https://doi.org/10.1002/2017GL073044.
Ying, Q., Kleeman, M.J., 2006. Source contributions to the regional distribution of secondary particulate matter in California. Atmos. Environ. 40, 736–752. https://doi.org/10.1016/j.atmosenv.2005.10.007.
Ying, Q., Mysliwiec, M.J., Kleeman, M.J., 2004. Source apportionment of visibility impairment using a three-dimensional source-oriented air quality model. Environ. Sci. Technol. 38, 1089–1101. https://doi.org/10.1021/es0349305.
Ying, Q., Lu, J., Allen, P., Livingstone, P., Kaduwela, A., Kleeman, M., 2008. Modeling air quality during the California regional PM10/PM2.5 air quality study (CRPAQS) using the UCD/CIT source-oriented air quality model - part I. Base case model results. Atmos. Environ. 42, 8954–8966. https://doi.org/10.1016/j.atmosenv.2008.05.064.
Yu, X., Venecek, M., Kumar, A., Hu, J., Tanrikulu, S., Soon, S.T., Tran, C., Fairley, D., Kleeman, M.J., 2019. Regional sources of airborne ultrafine particle number and mass concentrations in California. Atmos. Chem. Phys. 19, 14677–14702. https://doi.org/10.5194/acp-19-14677-2019.
Zapata, C.B., Yang, C., Yeh, S., Ogden, J., Kleeman, M.J., 2018a. Low-carbon energy generates public health savings in California. Atmos. Chem. Phys. 18, 4817–4830.

https://doi.org/10.5194/acp-18-4817-2018.
Zapata, C.B., Yang, C., Yeh, S., Ogden, J., Kleeman, M.J., 2018b. Estimating criteria pollutant emissions using the California Regional Multisector Air Quality Emissions (CA-REMARQUE) model v1.0. Geosci. Model Dev. 11, 1293–1320. doi:https://doi.org/10.5194/gmd-11-1293-2018
Zhang, Y., Qian, Y., Dulière, V., Salathé, E.P., Leung, L.R., 2012. ENSO anomalies over the Western United States: present and future patterns in regional climate simulations. Clim. Change 110, 315–346. https://doi.org/10.1007/s10584-011-0088-7.
Zhao, Y., Li, Y., Kumar, A., Ying, Q., Vandenberghe, F., Kleeman, M.J., 2022. Separately resolving NOx and VOC contributions to ozone formation. Atmos. Environ. 285, 119224. https://doi.org/10.1016/j.atmosenv.2022.119224.
Zhao, Y., Li, Yin, Li, Yiting, Kumar, A., Ying, Q., Kleeman, M.J., 2024. Reducing southern California ozone concentrations in the year 2050 under a low carbon energy scenario. Atmos. Environ. 320, 120315. https://doi.org/10.1016/j.atmosenv.2023.120315.